Reconstruction analysis of global ionospheric outflow patterns

Michael Liemohn[1], Jörg-Micha Jahn[2], Raluca Ilie[3], Natalia Y. Ganushkina[1,4], Daniel T. Welling[1], Heather A. Elliott[2], Meghan Burleigh[5], Kaitlin Doublestein[1], Stephanie Colon-Rodriguez[1], Pauline Dredger[1], and Philip W. Valek[2]

[1] Department of Climate and Space Sciences and Engineering, University of Michigan, Ann Arbor, MI, USA

[2] Southwest Research Institute, San Antonio, TX, USA

[3]Department of Electrical and Computer Engineering, University of Illinois, Urbana-Champaign, IL, USA

[4]Finnish Meteorological Institute, Helsinki, Finland

[5]Naval Research Laboratory, Washington, DC, USA

Corresponding author: Michael Liemohn (liemohn@umich.edu)

In preparation for/Submitted to *Journal of Geophysical Research Space Physics*

Key Points:

- A simulation study is conducted to determine the number of spacecraft needed for accurate reconstruction of 2D ionospheric outflow patterns
- Determining the global pattern of ionospheric outflow is needed to understand the geospace system, especially during geomagnetic storms
- A potential ionospheric outflow mission concept is defined that could address this unresolved key issue of space physics and space weather

AGU Index Terms:

- 2431 Ionosphere/magnetosphere interactions (2736)
- 2736 Magnetosphere/ionosphere interactions (2431)
- 2776 Polar cap phenomena
- 2788 Magnetic storms and substorms (4305, 7954)
- 2794 Instruments and techniques

Keywords:

ionospheric outflow, spaceflight hardware, space mission, magnetosphere-ionosphere coupling, ion composition, high-latitude ionosphere

Abstract

Ionospheric outflow supplies nearly all of the heavy ions observed within the magnetosphere, as well as a significant fraction of the proton density. While much is known about upflow and outflow energization processes, the full global pattern of outflow and its evolution is only known statistically or through numerical modeling. Because of the dominant role of heavy ions in several key physical processes, this unknown nature of the full outflow pattern leads to significant uncertainty in understanding geospace dynamics, especially surrounding storm intervals. That is, global models risk not accurately reproducing the main features of intense space storms because the amount of ionospheric outflow is poorly specified and thus magnetospheric composition and mass loading could be ill-defined. This study defines a potential mission to observe ionospheric outflow from several platforms, allowing for a reasonable and sufficient reconstruction of the full outflow pattern on an orbital cadence. An observing system simulation experiment is conducted, revealing that four well-placed satellites are sufficient for reasonably accurate outflow reconstructions. The science scope of this mission could include the following: reveal the global structure of ionospheric outflow; relate outflow patterns to geomagnetic activity level; and determine the spatial and temporal nature of outflow composition. The science objectives could be focused to be achieved with minimal instrumentation (only a low-energy ion spectrometer to obtain outflow reconstructions) or with a larger scientific scope by including contextual instrumentation. Note that the upcoming Geospace Dynamics Constellation mission will observe upwelling but not ionospheric outflow.

Plain Language Summary

Earth's upper atmosphere above 500 km altitude constantly loses charged particles to outer space in a process called ionospheric outflow. This outflow is important for the dynamics of the near-Earth space environment ("space weather") yet is poorly understood on a global scale. A mission is needed to observe the global patterns of ionospheric outflow and its relation to space weather driving conditions. The science objectives of such a mission could include not only the reconstruction of global outflow patterns but also the relation of these patterns to geomagnetic activity and the spatial and temporal nature of outflow composition. A study is presented to show that four well-placed spacecraft would be sufficient for reasonable outflow reconstructions.

1. Introduction

The Earth's ionosphere constantly loses material to deep space. This "ionospheric outflow" can be on the order of 10^{25} to 10^{26} ions/s, which is about 1-10 kg/s (e.g., Moore et al., 1997). This outflow is not steady but rather reacts to changes in the solar EUV photon flux striking the upper atmosphere, as well as to the electromagnetic driving from the solar wind after it has been processed through Earth's magnetosphere. A pivotal feature of intense space storms is a change in near-Earth plasma composition from a dominance of protons (e.g., Lui & Hamilton, 1992; Pulkkinen et al., 2001) to heavy ions like O^+ that flows out of Earth's ionosphere at these times (e.g., Chappell et al., 1987; Young et al., 1982). The ionosphere essentially supplies most of the heavy ions that exist in many parts of the magnetosphere (all except for He^{2+}, which originates in the solar wind), such as to the lobe, the plasma sheet, in the far tail, and even to the magnetosheath (Hamilton et al., 1988; Christon et al., 2000, 2002; Mall et al., 2002; Liu et al., 2005; Kistler et al., 2010a, c; Mouikis et al., 2010;). Figure 1 is an artist's rendering of ionospheric outflow, shown here as being dominated by outflow from the cusp (as found by, e.g., Moore et al., 1999a; Lund et al., 2018) with many of the ions escaping into the magnetotail lobes. Seki et al. (2015) provides an excellent review of the processes leading to outflow and Welling et al. (2015b) is a comprehensive examination of the fate of this outflow throughout geospace.

The presence of heavy ionospheric-origin ions in the magnetosphere has multiple influences including the following: enhance system inertia; lower the Alfvén speed; modify plasma turbulence; control micro-processes like reconnection; and slow the system response time to disturbances. Given the significance of these effects, a number of global magnetospheric fluid models (often magnetohydrodynamic, or MHD, codes) have incorporated them to some extent (e.g., Winglee et al., 2002, 2009; Glocer et al., 2009a, b;

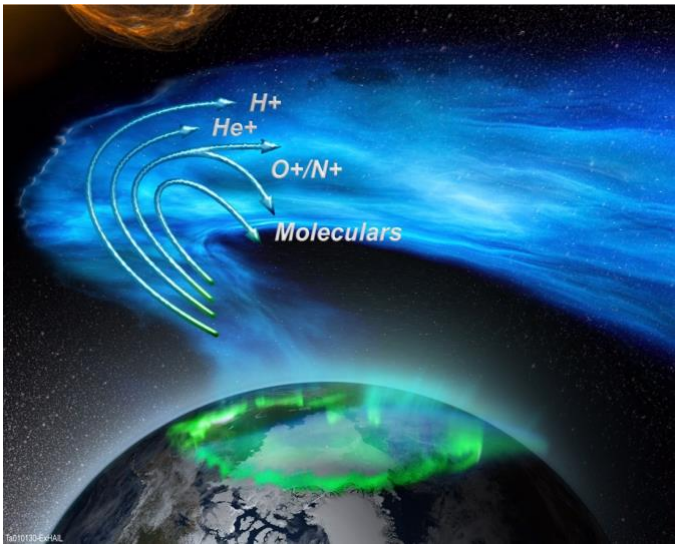

Figure 1. Artist's concept of high latitude ionospheric outflow.

Brambles et al., 2010, 2011; Garcia et al., 2010; Wiltberger et al., 2010; Welling et al., 2011; Ilie et al., 2013, 2015; Liemohn and Welling, 2016). Results from these multifluid simulations show that the presence of heavy ions may slow the magnetospheric convection, reduce the cross-cap potential, influence the dayside reconnection, alter the behavior of the plasma sheet, stimulate substorms, and magnify the storm time Dst. MHD models with ionospheric outflow as an inner magnetospheric boundary condition do not include known kinetic physics effects, though, and such models typically adopt either uniformly distributed outflow or localized (usually near the cusp) upflowing ion fluxes computed, often, from the Strangeway et al. (2005) model. The Strangeway relationship, however, is derived from relatively limited observational data and therefore suffers from several severe drawbacks. For instance, the predicted flux does not depend on season, solar activity, or local time, or universal time. The solar activity needs to be included to reproduce the amount of ionization at lower altitudes – that is, the supply of ionospheric ions available for outflow. Moreover, this model does not include a specification of density, velocity, and temperature needed as boundary conditions for the MHD simulations; only outflow flux is provided by the Strangeway relationship.

Global magnetospheric MHD models reveal that this outflow mass loads the magnetosphere, leading to reactive feedback processes and emergent phenomena not seen during quiescent times (e.g., Wiltberger et al., 2010). However, such global models do not accurately reproduce the observed Dst time series during intense space storms because the global dynamics and amount of ionospheric outflow are only poorly characterized. Figure 2 shows results from the "Dst challenge" (Rastätter et al., 2013), in which several global models were used to reproduce Dst for several very different storms (four shown here). Each model produced dramatically different results, with some codes overestimating the depth of Dst and others barely registering any Dst signature. While the grid resolutions and numerical solvers play a role in these differences, a key critical input is the ionospheric outflow setting, as illustrated by the widely different results even from the same model.

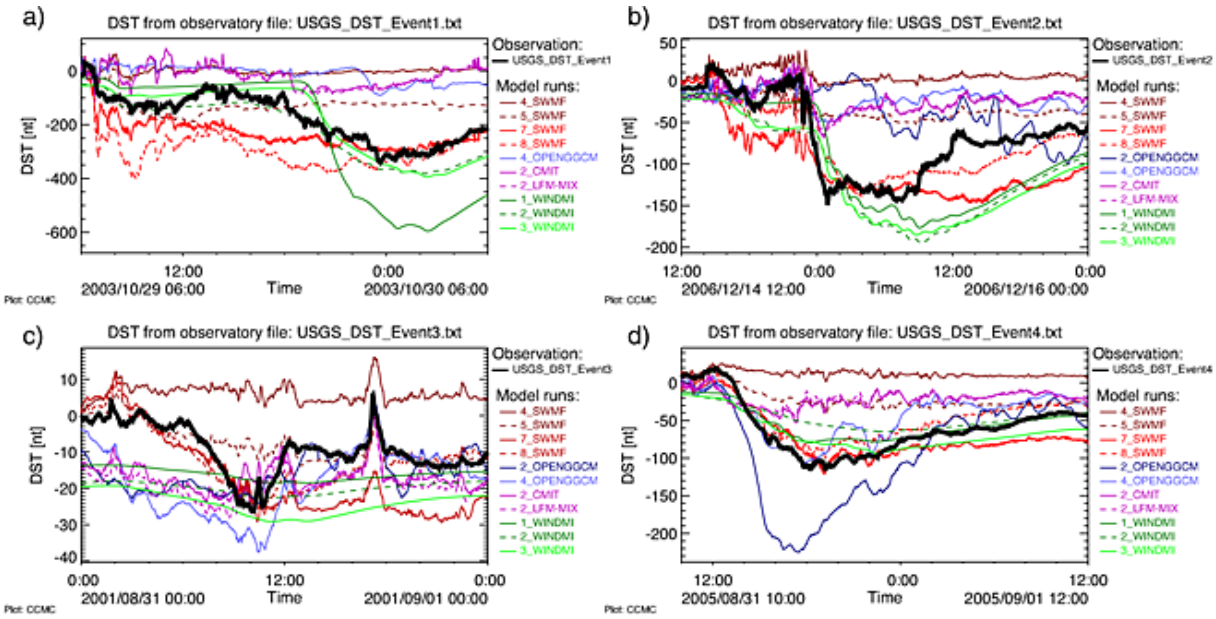

Figure 2. From Rastätter et al. (2013), Dst data-model comparison from several global models of 4 storm events. One of the reasons that the simulation results are so different from each other, even from the same model, is the assumed ionospheric outflow specification.

Modeling alone cannot properly quantify the global outflow patterns. An in situ mission is needed that would discover how Earth's ionosphere dynamically and globally feeds plasma to its magnetosphere by quantifying the ionospheric outflow intensity, composition, and acceleration variability over both regional and global scales. Some of the ionospheric outflow escapes directly into deep space, but much of it initially circulates within the magnetosphere. This extra mass and dissimilar motion (e.g., the vastly different gyroradii of light and heavy ions) alters the dynamics of the magnetic field, it slows down plasma flow speeds, and it changes the global interaction of the solar wind with the magnetosphere. It can even influence future ionospheric outflow rates. As a result, a natural feedback loop exists. Solar wind conditions govern the outflow, which mass loads the magnetosphere and in return modifies the nature of how the solar wind regulates outflow. Present knowledge of these processes only reveal the spatial structure of the high-latitude ionospheric outflow through long-term statistical compilations of single-spacecraft missions. This is inadequate for describing and fully understanding the dynamics of this feedback system. A mission to measure global ionospheric outflow – in conjunction with upstream measurements of solar wind driving conditions from

other spacecraft – would examine this nonlinear connection with multi-point observations leading to large-scale reconstructions of the ionospheric outflow pattern.

2. The need for additional investigation

The polar wind and energetic ion outflow processes have been studied for more than forty years via a variety of both experimental and modeling techniques (cf. reviews by Banks & Holzer, 1968; Moore, 1984; Moore and Delcourt, 1995; Ganguli, 1996; Yau et al., 1997; Hultqvist et al., 1999; Yau et al., 2007; Moore & Horwitz, 2007; Schunk and Nagy, 2009; Moore and Horwitz, 2009; Kronberg et al., 2014; Wiltberger, 2015). Past missions – such as the International Satellites for Ionospheric Studies (ISIS), in particular ISIS-1 (e.g., Brinton et al., 1971; Hoffman & Dodson, 1980), or the Dynamics Explorer satellites, notably DE-1 (e.g., Gurgiolo & Burch, 1982; Nagai et al., 1984, Chandler et al., 1991), as well as Akebono (e.g., Abe et al., 1993; Yau et al., 1995), Polar (e.g., Su et al., 1998b; Moore et al., 1999a, b; Liemohn et al., 2005, 2007), the Defense Meteorological Satellite Program (DMSP) spacecraft (e.g., Coley et al., 2003); the Fast Auroral SnapShoT (FAST) mission (e.g., Strangeway et al., 2000, 2005), and the Cluster mission (e.g., Kistler et al., 2010a; Liao et al., 2015; Dandouras, 2021) – have observed ionospheric outflow with one or two spacecraft. Sometimes these are well-instrumented to observe energy input and ionospheric outflow response, leading to input-outflow correlations. Based on this work, the basic physics of outflow of thermal plasma from the terrestrial ionosphere at high latitudes is well known. Figure 3 shows a schematic that summarizes the major processes of outflow. Shown here are Joule heating in the thermosphere and ionosphere (e.g., Foster et al., 1983; Gombosi & Killeen, 1987; Pollock et al., 1990; Liu et al., 1995), ponderomotive or transverse ion acceleration by plasma waves (e.g., Whalen et al., 1991; Miller et al., 1995; Lundin & Guglielmi, 2006), acceleration by parallel electric fields (e.g., Cladis, 1986; Schunk, 2000; Chaston et al., 2016), and high-altitude centrifugal energization (e.g., Horwitz et al., 1994; Demars et al., 1996; Winglee, 2000). Various populations of energetic electrons are also possible channels for heating or accelerating ions to escape velocities, such as atmospheric photoelectrons (e.g., Lemaire, 1971; Khazanov et al., 1997; Tam et al., 2007; Glocer et al., 2017), polar rain (e.g., Waite et al., 1985; Wilson et al., 1997; Su et al., 1998a), and soft electrons in the dayside cusp (e.g., Nilsson et al., 1994; Valek et al., 2002; Fuselier et al., 2003;

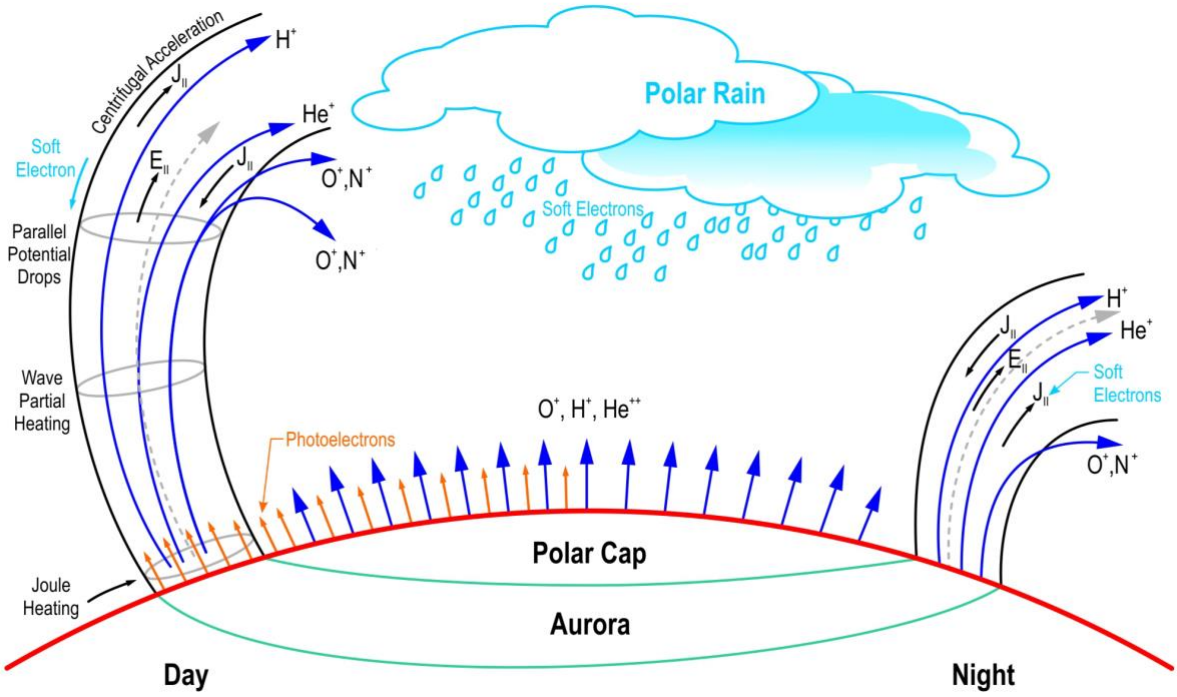

Figure 3. Schematic of physical processes contributing to ionospheric outflow.

Yizengaw et al., 2006; Wiltberger et al., 2010) or nightside auroral zone (e.g., Wahlund et al., 1992; Richards, 1995; Barakat et al., 1998; Wu et al., 1999; Lynch et al., 2007; Zeng & Horwitz, 2007).

As the outflowing ions drift through the different regions (e.g., Elliott et al., 2007), the plasma is energized by mechanisms that operate with different levels of intensity at different altitudes and in different high-latitude regions. Most of the outflow comes from the dayside cusp and nightside auroral zones. A particularly difficult confounding element, however, is the transit of upflowing ions from the topside ionosphere to higher altitudes where additional acceleration converts these populations into outflow. That is, observed outflow can be related to energization processes, but the spatial distribution of outflow is only known statistically or from numerical modeling. The inherent time delay in the outflow process obscures correlations between driving factor and outflow intensity.

Figure 4 shows two ionospheric outflow patterns (of ion radial velocity), from Akebono measurements (Abe et al., 2004) and from numerical modeling (Glocer et al., 2012). The

observed pattern was assembled from many years of data, yet it still reveals significant meso-scale structure in the outflow pattern. This is most likely due to statistical noise as the radial velocity changes considerably from pass to pass. The modeled pattern has several features in common with the statistical pattern, including meso-scale patches of intense outflow speeds, but other aspects are not the same. For a global modeling simulation of a particular event, it is not fully adequate to use either of these approaches for the outflow specification, leading to uncertainty in the magnetospheric fate and consequences, introducing a large caveat to any large-scale geospace simulation study and the analysis and prediction of space weather.

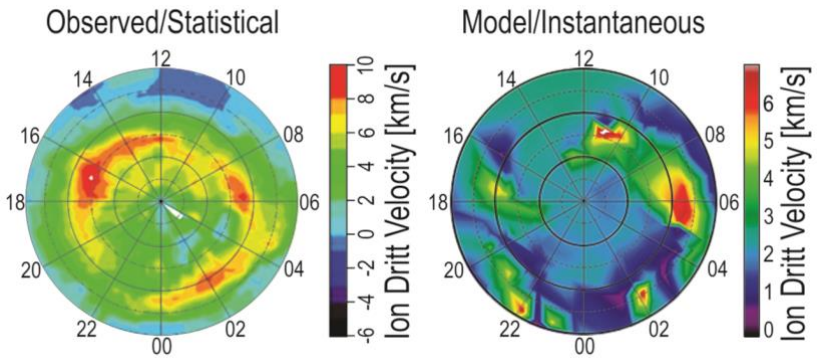

Figure 4. Examples of the spatial complexity inherent in O^+ outflow velocity in the polar (>60° invariant latitude) ionosphere. The left frame is constructed from nearly a decade of Akebono satellite observations (Abe et al., 2004), yet still shows a highly structured outflow pattern. The right frame is constructed from Polar Wind Outflow Model (adapted from the results of Glocer et al., 2012) when 392 flux tubes are simulated under moderate solar driving. Note that the two colorscales are different.

Importantly, the current statistically-known spatial structure does not reveal the dynamics of outflow. While *in situ* measurements have revealed important statistical properties of ion outflow, measurements are made at a given magnetic local time (MLT) and altitude. Since they are taken over some period of time (a few minutes), it does not allow the determination of the temporal and spatial variation of ion outflow in response to variable solar wind and interplanetary magnetic field (IMF) conditions during the progression of geomagnetic storms. As argued by Liemohn et al. (2022), it is important to understand event-specific spatial and temporal variability in order to quantify the impact of outflow on the geospace system. The community lacks this capability with respect to the structure of outflow for any particular disturbed time.

All of this uncertainty about the spatial pattern of outflow consolidates in our estimates of fluence, or the global outflow rate from the ionosphere into the magnetosphere. Currently,

fluence is estimated only to order-of-magnitude accuracy (Yau et al., 1988; Cully et al., 2003; Lennartsson et al., 2004). All estimations are based on statistical studies from single-spacecraft missions. Estimates from models vary wildly (e.g., Welling et al., 2016), providing limited insight on the true value. After decades of investigations, we still cannot confidently state the spatial distribution and amount of ionospheric plasma that enters the magnetosphere.

Note that the upcoming Geospace Dynamics Constellation (GDC) mission is not designed to achieve the objective considered here of a global map of ionospheric outflow. While the payload of its six spacecraft includes a low-energy ion instrument, its target altitude below 400 km is significantly too low for the task proposed here. That is, it might see ionospheric *upwelling*, but does not distinguish the portion that becomes ionospheric *outflow*. Much of the acceleration for heavy ions to reach escape velocity occurs at higher altitude than where GDC will be located. To observe outflow, the satellite should be, at a minimum, above 1000 km, and 2000 km would be even better to ensure that most of the ions have reached escape velocity and are therefore actually leaving the atmosphere.

3. Potential science objectives of this mission

There are three main science objectives that should be targeted for a mission devoted to observing the pattern of high-latitude ionospheric outflow:

- Reveal the global structure of ionospheric outflow
- Relate outflow patterns to solar wind driving and geomagnetic activity
- Determine the spatial and temporal nature of outflow composition

An ancillary modeling task that should be associated with this mission is mapping the outflow through the magnetosphere and connecting the outflow patterns to any available relevant measurements elsewhere in geospace.

3.1. Reveal the global structure of ionopsheric outflow

Ionospheric outflow is a time-varying source of plasma for the near-Earth space environment. Outflow forms complex and spatially detailed patterns. The composition, magnitude, and spatial distribution of outflowing fluxes vary strongly as a function of solar and magnetospheric activity. Outflowing plasma feeds the magnetosphere, playing a role in almost

all global processes. In order to understand magnetospheric dynamics, it is critical to understand the complicated and non-linear dynamics of outflow. Ionospheric outflow is a mosaic of many different populations, creating a complicated spatial structure that cannot be captured by single-spacecraft missions.

Ionospheric outflow organizes into distinct regions, including polar cap, auroral zone, and cusp outflow. Nested within these regions are distinct populations, such as bulk cold outflows with temperatures below 1 eV and suprathermal flows (10 eV up to low keV), such as ion beams and conics. The distributions are highly non-Maxwellian, forming pancake, conic, toroid, bi-Maxwellian, double-peaked, counter-streaming, and elongated-tail distributions (Andre and Yau, 1997; Schunk and Nagy, 2009). These flows contain both light and heavy ions: H^+, He^+, N^+, and O^+. While outflow regions can be expansive (e.g., the polar cap), they are often localized and overlapping (Giles et al., 1994; Abe et al., 2004). Of particular interest is the cusp, which is limited in area (typically a few hundred kilometers in any direction at ionospheric altitudes, as found by Newell and Meng (1994)), but yields strong outflowing fluxes to the magnetosphere (Lockwood et al., 1988; Kistler et al., 2010b). Meso-scale outflow "hotspots" also exist, with spatial scales of several hundred kilometers. Figure 4 shows different illustrations of the complex spatial pattern, both statistically observed (left panel) and simulated (right panel). Both large and meso-scale outflow features are apparent in both panels of Figure 4. The characteristics of each outflow population, including energy, pitch angle, and source location, all determine how that population will be transported into and throughout the magnetosphere (Delcourt et al., 1989; Cully et al., 2003; Huddleston et al., 2005).

Beyond an understanding that this complexity exists, we know little concerning the global distribution of specific ionospheric outflow populations. Coarse maps are constructed statistically using single-spacecraft observations aggregated over long periods (Abe et al., 2004; Peterson et al., 2006). These studies yield only an initial idea of flux distributions. When segregated by energy or distribution shape, the available statistics are too low to be useful. Though strong east-west oriented IMF can drive pronounced interhemispheric asymmetries in ionospheric dynamics (e.g., Weimer, 2001a, b), such asymmetries are rarely considered in outflow because of observation limitations, particularly in the southern hemisphere.

3.2. Relate outflow patterns to geomagnetic activity level

Compounding the spatial complexity of outflow is its temporal nature. Outflow regions follow the magnetospheric geometry: as the cusp (e.g., Farrell and Van Allen, 1990; Fung et al., 1997; Zhou et al., 2000; Pitout et al., 2006) and auroral oval move as a function of solar driving and magnetospheric activity, and corresponding ionospheric plasma sources. Many acceleration processes are also the result of energy inputs from the solar wind and magnetosphere. This results in outflow patterns that are tied not only to the solar cycle (e.g., Yau et al., 1985, 1998; Abe et al., 2004), but also to specific solar wind conditions (Lennartsson et al., 2004; Elliott et al., 2001; Cully et al., 2003), geomagnetic storm phase (Nosé, et al., 2003; Moore et al., 1999; Kitamura et al., 2010), and magnetospheric transients, such as substorms (Øieroset et al., 1999; Wilson et al., 2004; Kistler et al., 2006). The resultant outflowing fluxes at 2000 km altitude vary from 1×10^5 $cm^{-2}s^{-1}$ to 5×10^8 $cm^{-2}s^{-1}$ as a function of season, species, and geomagnetic and solar activity (Yau et al., 2007).

Single satellite missions have not been able to resolve time dynamics of outflow. Statistical studies can only quantify outflow variability via total fluence as a function of simple indices (Yau et al., 1988) or binned by average solar wind conditions (Cully et al., 2003). Such studies cannot illustrate important details across storm timescales. What outflow regions and populations are most prominent during different storm phases? How does outflow compare between different types of storms, such as coronal mass ejection (CME) or corotating interaction region (CIR) driven events? How does the occurrence, size, and intensity of outflow hotspots depend on storm phase and intensity? These questions cannot be answered with traditional, single-point measurements, limiting our understanding of how dynamic outflow affects the active magnetosphere.

Researchers cannot understand the highly time dynamic nature of ionospheric outflow without frequent, distributed observations. This mission concept would provide these measurements and solve the question about how outflow evolves over the course of a geomagnetic storm.

3.3. Determine the spatial and temporal nature of outflow composition

The proposed mission should have the capability to separately measure the outflowing plasma population and identify its major constituents. Measuring composition provides an avenue to distinguish between energization and transport mechanisms (e.g., Ilie and Liemohn, 2016). For instance, in spite of only 12% mass difference, nitrogen and oxygen have different ionization energies (15.6 eV and 12.1 eV respectively) as well as different scale heights (Chappell et al., 1982). The cross section for charge transfer between atomic hydrogen and nitrogen ions is significantly different than the cross section for charge transfer between atomic hydrogen and oxygen ions (Stebbings et al., 1960). Because the peak production rates for those two ionospheric heavy ions usually happen at different altitudes, their abundance in the outflow serves as a tracer for the altitude dependent energization processes. Theoretical studies predict significant densities of N^+ (e.g., Schunk and Raitt, 1980; Sojka et al., 1982; Lin et al., 2020; Lin and Ilie, 2022), showing a strong dependence on diurnal, seasonal, and geomagnetic activity as well as universal time.

Since the production of N^+ increases with increased energy input, it is expected that it is more prevalent in the auroral regions. Observation of enhanced N^+ fluxes outside the auroral region would reveal new insight into latitudinal transport of heavy ions and consequently the overall ionospheric dynamics. Because the mass distribution of accelerated ionospheric ions reflects the source region of the low altitude ion composition, any measurement of a minor ion constituent of the accelerated plasma serves as a tracer of ionospheric and energization processes (e.g., Winningham & Gurgiolo, 1982; Glocer & Daldorff, 2022). Ion velocity space measurements alone reveal the basic breakdown of these processes, separating classic polar wind (heating only, allowing the high-energy tail to escape) from potential-driven outflow (various $E_{||}$ contributions) and wave heating (transversely accelerated ions and conics).

Enhancement of ion outflow is also associated with an increase in the solar wind dynamic pressure (Moore et al., 1999a; Elliott et al., 2001; Cully et al., 2003; Ogawa et al., 2009) and in the solar wind electric field (Lennartsson, 1995; Elliott et al., 2001). The amount of outflowing ion flux and the interplay between different energization mechanisms are largely governed by changes in the solar wind density, velocity, and IMF because it is these parameters that control the precipitation into the ionosphere and the convection electric field (Moore and Horwitz,

2007). Furthermore, the enhancement of ionospheric outflow becomes larger with increasing geomagnetic activity as the auroral oval (where the largest ionospheric outflow occurs) moves equatorward (Ogawa et al., 2009). At higher altitudes, the curvature of the magnetic field in the polar cap produces a centrifugal acceleration of the convecting plasma and this effect becomes important during times of strong convection. However, centrifugal acceleration affects predominantly the lowest energy ions by increasing their parallel velocity (Cladis, 1986). To measure outflow, the satellites should be above the acceleration region that pushes them above escape velocity (at least 1000 km altitude, and perhaps much higher).

3.4. Map outflow throughout the magnetosphere

Our understanding of outflow's role throughout the magnetosphere is tempered by our tenuous understanding of outflow itself. A combination of global outflow observations with numerical modeling is necessary to completely reveal how ionospheric outflow maps throughout the magnetosphere.

An example of this is presented in Figure 5. The main graphic shows trajectory traces of H^+ and O^+ ions through a multifluid global simulation that resolves velocities for each ion species. It is seen that the locations of initial contact with the plasma sheet are vastly different for the two species, which could modify magnetotail dynamics. The inset in Figure 5 shows the "fate" of ionospheric outflow as a function of initial location within the high-latitude ionosphere. This is similar to the fate maps from Huddleston et al. (2005), except that, instead of an empirical field description, this uses results from an MHD model (Gombosi et al., 2021; with setup like that of Liemohn & Welling, 2016, and Glocer et al., 2018). For this particular model configuration and driving condition (nominal southward IMF), a pattern can be obtained revealing which ionospheric locations contribute to which magnetospheric regions.

The temporal and spatial complexities of ionospheric outflow propagate through the magnetosphere, affecting system-level dynamics. Observations paint a clear dependence between solar wind/magnetospheric activity and heavy ion composition in the magnetosphere. In the lobes, different populations disperse by energy and species (Chappell et al., 1987). O^+ beams from the cusp distinguish themselves from isotropic nightside auroral O^+ (Kistler et al., 2010b; Liao et al., 2010; Kistler et al., 2016). Very cold ion populations indicate cold, classical polar wind outflow (Engwall et al., 2009; Andre et al., 2015). Faster populations can escape the

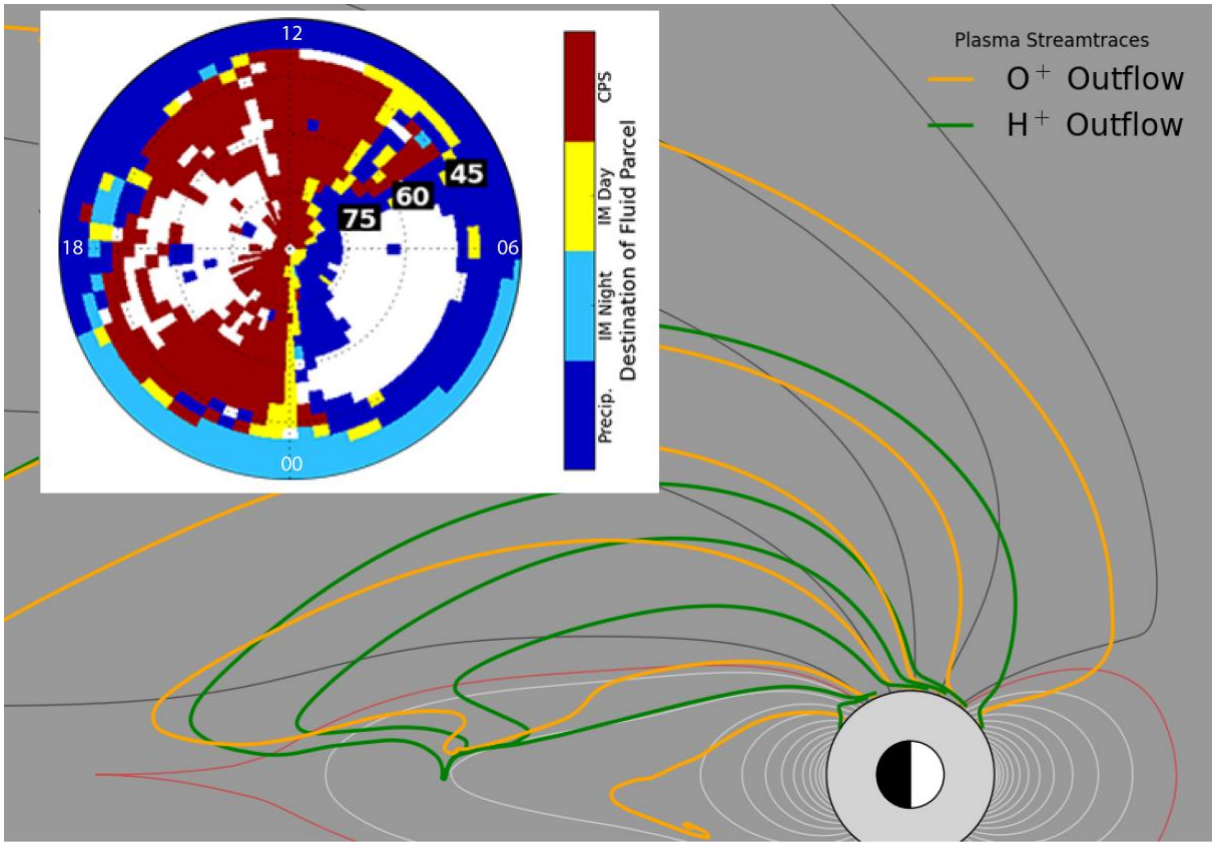

Figure 5. Streamline traces of ionospheric outflow from 5 locations on the model inner boundary along the noon-midnight meridian in the northern hemisphere (view is from dawn). The orange curves are for O^+ and the green curves are for H^+. The thin white lines show closed magnetic field lines and the thin red lines are the last closed field lines on the dayside and nightside. The inset panel shows the fate of mapping outflow from a starting grid in the northern hemisphere (noon at the top), with their first crossings of the equatorial plane indicated by color: central plasma sheet (red); dayside inner magnetosphere (yellow); nightside inner magnetosphere (light blue); precipitation back into the model inner boundary (dark blue); and loss to deep space (white).

geospace domain all the way to deep space, while slower (and typically heavier) populations arrive at the plasma sheet (Young et al., 1982; Lennartsson and Shelley, 1986; Moore et al., 2005a, b; Nosé et al. 2005; Mouikis et al., 2010). Here, they are accelerated sunward, feeding the partial and symmetric ring current hot ion populations (e.g., Gloeckler et al., 1985; Daglis et al., 1999; Denton et al., 2005). Figure 6 (from Nosé et al., 2003) shows the energy density ratio in the inner magnetosphere and near-Earth plasma sheet, between O^+ and H^+ (in red) and between He^+ and H^+ (in blue). In these ratios, the numerator species is supplied only by the ionosphere while protons could be sourced from either the ionosphere or the solar wind. It is clear that the

energy density of the ring current becomes increasingly carried by O^+ as a function of storm intensity.

Although ionospheric outflow is a major source of magnetospheric plasma, recent studies suggest a more complicated connection. Numerical models have repeatedly demonstrated that the characteristics of outflow at its source, including mass, pitch angle, and energy, help dictate the fate of the plasma inside the magnetosphere (Huddleston et al., 2005; Brambles et al., 2010; Garcia et al., 2010; Yu and Ridley, 2013a, b). Within the plasma sheet, characteristics like composition, distance down tail, and pitch angle distribution dictate the amount of acceleration of the plasma (Delcourt et al., 1989, 1993; Kronberg et al., 2012). The characteristics of outflow throughout the plasma sheet control how effectively it will energize the ring current (e.g., Welling et al., 2011). Further, as outflow affects magnetospheric dynamics, such as substorm development (Wiltberger et al., 2010; Welling et al., 2016) and cross polar cap potential (Winglee et al., 2002; Welling and Zaharia, 2012; Ilie et al., 2013, 2015), it is also affecting the energy input into the ionosphere, creating non-linear magnetosphere-ionosphere feedback loops (Moore et al., 2014; Welling and Liemohn, 2016). These have been linked to sudden ring current intensifications (Welling et al., 2015a) and the development of global sawtooth oscillations (Brambles et al., 2011, 2013). The geopauses – those surfaces in near-Earth space where the contribution from solar and ionospheric origin plasma are equal (in density, mass, or pressure) – are boundaries that define changes in the physical processes governing plasma flow (e.g., Trung et al., 2019; 2023). The community now recognizes that magnetospheric dynamics rely critically on outflow dynamics.

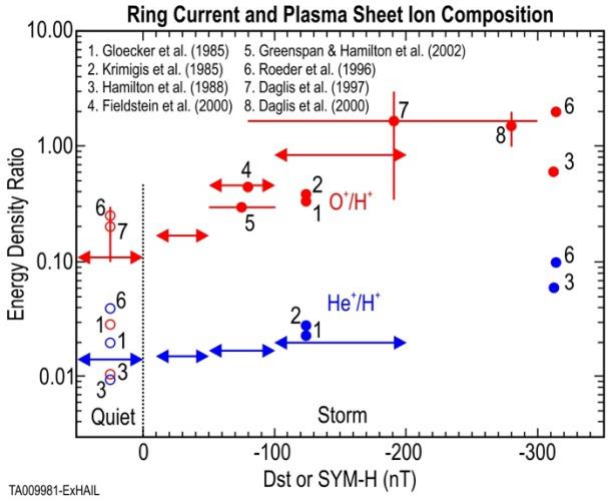

Figure 6. The energy density ratio between O^+ and H^+ (in red) and between He^+ and H^+ (in blue) of the ring current and plasma sheet as a function of geomagnetic activity, as indexed by Dst or SYM-H (Nosé et al., 2003). Note the logarithmic scale on the y axis.

The source of most of the uncertainties regarding geospace dynamics are caused by the limitations of our current understanding of the spatial and temporal variation of ionospheric outflow. Observational studies of ion composition in geospace must rely on inference to connect

the source population to the magnetospheric observations (e.g., Kistler et al., 2016). Numerical simulations depend on the inherently flawed statistical outflow distributions to seed models, propagating error throughout the magnetosphere (e.g., Huddleston et al., 2005; Peroomian et al., 2006). Scientists are simply unable to definitively answer critical questions connecting outflow and the magnetosphere.

4. Determining the optimal number of spacecraft

While it would be ideal to know ionospheric outflow everywhere at all times, this would require a Starlink-level constellation of hundreds of satellites. Instead, there is a trade space of cost versus reconstruction accuracy that needs to be assessed to determine the optimal number of spacecraft that would provide reasonable reconstructions most of the time. Therefore, an observing system simulation experiment is useful to provide some constraints on the constellation configuration.

This exploration was conducted using several existing outflow patterns, represented here by results from a high-resolution single-fluid MHD simulation, specifically those from Welling & Liemohn (2014). For more on the numerical code, please see the latest summary of the Space Weather Modeling Framework (SWMF) (Gombosi et al., 2021). Using values extracted from the original outflow pattern, a reconstruction is generated from these "observations" through binning and interpolation. Each virtual spacecraft takes 401 samples per orbit per hemisphere. These values are then sorting into 51 eually-spaced latitude bins per hemisphere and each latitude ring of values are then interpolated into 45 equally-spaced longitude bins using the Piecewise Cubic Hermite Interpolating Polynomial (PCHIP; Fritsch and Carlson, 1980). The PCHIP method conducts a cubic spline fit on a one-dimensional data set (in this case, the extracted outflow fluxes for a specific latitude band), with an extra filter that blends in linear interpolation to both preserve monotonicity of the resulting reconstruction and minimize overshoots near steep gradients within the data. The result is continuous but not necessarily smooth.

Latitudes above the available data are pruned, leaving an unreconstructed region at the pole. The reconstruction is a function of the number of satellites, the inclination of the orbit crossing point from the geomagnetic pole, the magnetic local time of the orbit crossing point, and the longitudinal separation of the orbit planes. Two solar wind input conditions (IMF

northward and southward) are used for the statistical study, and a time series of driving conditions are used for a real-event case study.

4.1. Example reconstruction patterns

Figure 7 illustrates the product of the reconstruction algorithm. For this example, the MHD result was produced using steady driving with an IMF Bz of -10 nT, taken from the simulation at 3 R_E geocentric distance (the inner boundary of the MHD model was set at 2.5 R_E) and mapped down to 1800 km altitude using flux conversation along assumed dipole field lines. For this reconstruction, three satellite passes were used with a crossing at 80˚ at local dawn (the sun is to the right in each of the plots), with a nodal separation of the orbit planes of 60˚. While some meso-scale outflow features are missed because an orbit plane did not pass through them, the overall pattern in the reconstruction is qualitatively similar to that of the original. Listed at the top of the original and reconstructed outflow maps is the total escaping ion fluence, which are only ~1% different.

To assess the appropriateness and quality of the selected reconstruction method, Figure 8 shows a PCHIP fit at the highest latitude band from the example in Figure 7. The red dots are the extracted data values. Because this is the highest latitude band, the satellite trajectories are moving on a very shallow arc (i.e., nearly horizontally) through the band, so even though there are only three satellites, each one contributes many points to the reconstruction. To enforce periodicity of the reconstruction, the data are repeated three times within to ensure continuity of the fit at ±180˚. The PCHIP result is shown in blue. Figure 8 shows that the PCHIP algorithm is excellent at reconstructing the functional form of the data in regions where data exists, while also

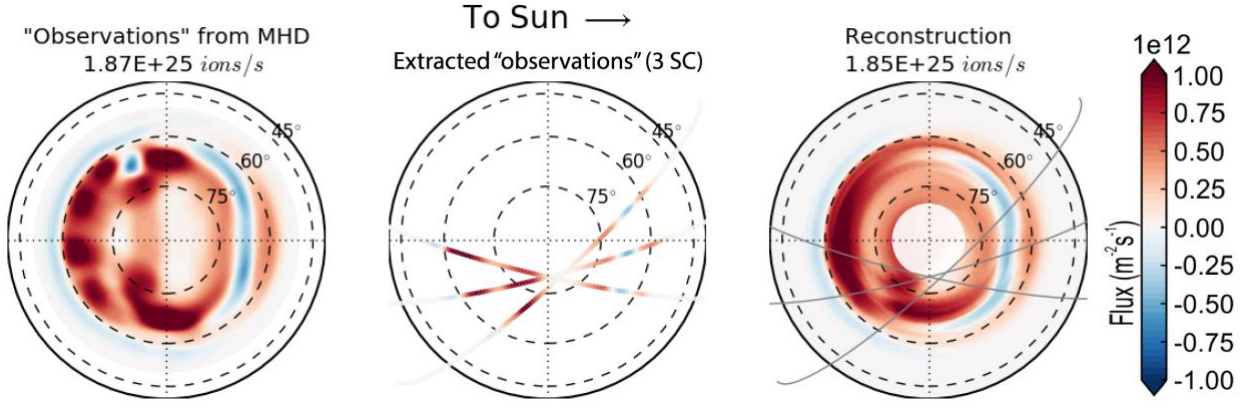

Figure 7. From a given outflow pattern (left), several satellite-pass extractions (center) are used to generate a reconstructed outflow pattern (right).

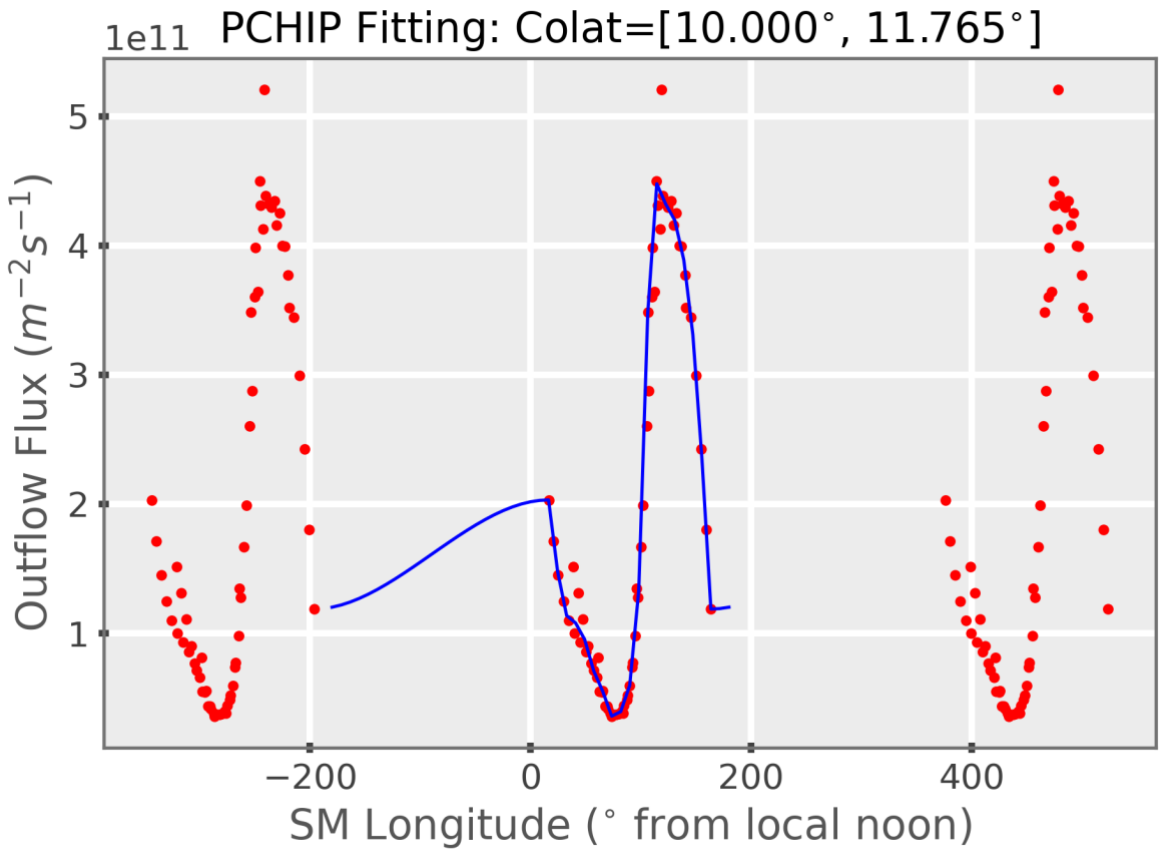

Figure 8. Example of a PCHIP fitting calculation of outflow flux as a function of longitude at a specific latitude band, specifically the highest latitude ring of the reconstruction example shown in Figure 7. The red dots are the MHD values extracted as "observations" within a particular colatitude band, repeated three times to ensure continuity of the fit. Values from the The blue curve is the PCHIP reconstruction.

creating a smooth curve through regions with no data points. It also does not introduce any new extrema beyond the observed maximum and minimum values.

Extending this example, Figure 9 shows reconstructions of that same MHD outflow pattern using one through five spacecraft passes for the reconstruction. To provide a different example from that shown in Figure 7, the crossing location in Figure 9 is at 85˚ at local midnight and the maximum orbit plane separation is set to 90˚. The reconstruction with a single spacecraft marginally reproduces a few of the global features but none of the meso-scale hotspots of outflow. This is to be expected as there are only two extracted values for each latitude ring, so each band in the reconstruction has a rather sinusoidal form. With two spacecraft, the global pattern is better, but the local features are still missing. Although patterns created from two or

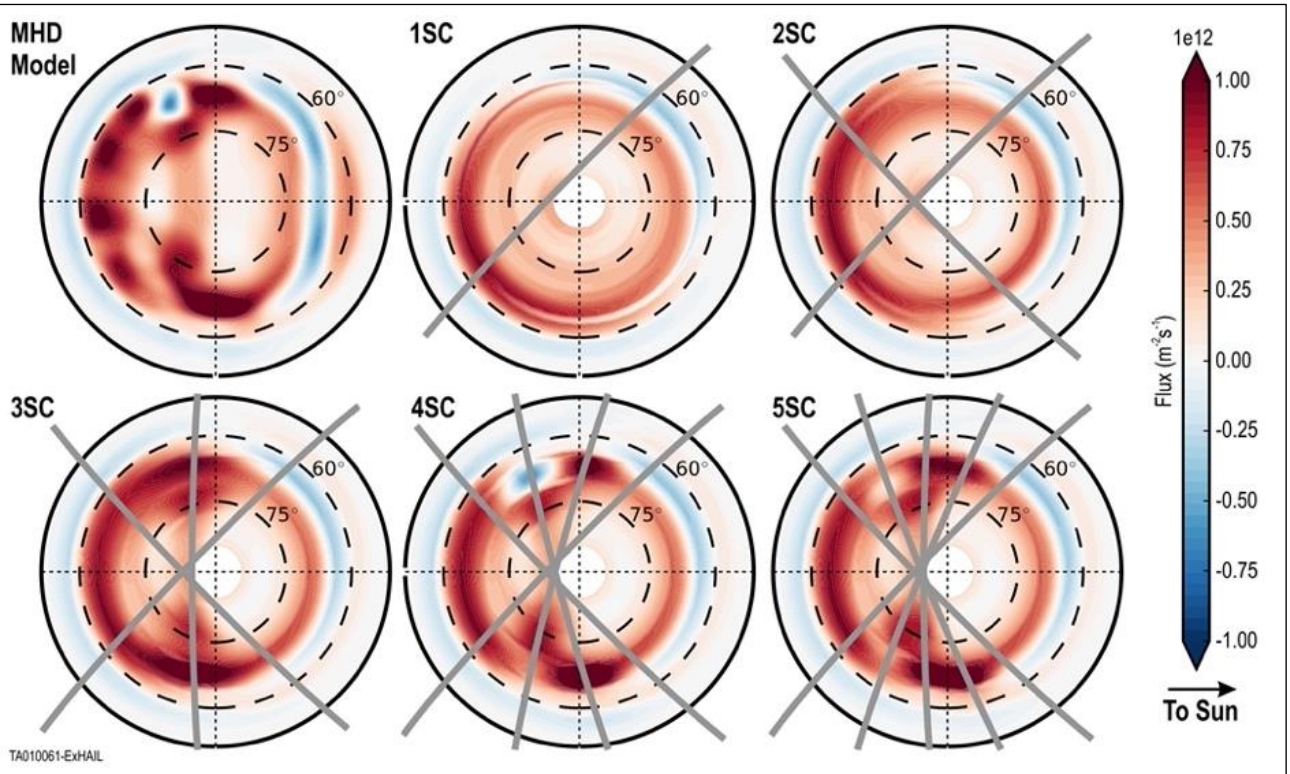

Figure 9. Reconstruction from a known spatial pattern of ionospheric outflow (upper left) using one through five spacecraft passes.

one spacecraft capture the large-scale features, these patterns reproduce essentially none of the localized outflow peaks and troughs. The pattern from three spacecraft is good but lacks some of the details of the hot spot structure within the outflow map. With four or five spacecraft, the localized features become resolved. Furthermore, it is seen that the interpolated pattern from four spacecraft is quite similar to that from five spacecraft.

4.2. Outflow reconstruction optimization

To quantify this, goodness of fit values for the 2D outflow map reconstructions were produced for constellations of one to six satellites. To further explore different mission phases, reconstructions were made using different orbit geomagnetic inclinations (from 65˚ to 90˚ in 5˚ increments), azimuths (i.e., local time) of orbit crossing points (full 360° at 14.4° increments) and spread of orbit planes (from 2° to 100° between the most distant satellites, in 10 settings, with any additional satellites above two equally spaced between these end members of the set). In all, over 10,000 spatial reconstructions were produced per MHD outflow spatial pattern plot.

For the results in this section, two such MHD patterns are considered, for a southward and northward IMF condition. These were taken from Welling & Liemohn (2014) from single-fluid MHD simulations. As seen in the first panels of Figures 7 and 9, the large-scale features of these initial ionospheric outflow patterns consist of outflow from the auroral oval (around all local times with a latitudinal extent of 5-10˚) with embedded "hot spots" of higher-intensity outflow flux (spanning 1-2 hours in local time and 3-5˚ in latitude). These are the scale of the features for which the reconstruction is being optimized.

The quality of reconstruction was then quantified. The fluxes at each latitude and longitude were compared between the reconstruction and the original pattern, resulting in a scatterplot of these paired values. This scatterplot was distilled to metric scores using root-mean-squared error (RMSE) and correlation coefficient (R), comparing each point within the reconstruction to the same point in the original outflow map. While two metrics are not enough for a robust analysis, these particular two metrics are from the accuracy and association categories (see, e.g., Liemohn et al., 2021) and provide a balanced overview of the goodness of fit between the patterns. This is only an initial conceptual study assessing the trade space between constellation configuration and reconstruction accuracy; a more thorough investigation of parameter space should be conducted for specific flight opportunities to justify the concept for that particular mission.

These two metrics are shown as a function of the number of satellites in Figure 10. These box-and-whisker plots were compiled using all combinations of the other inputs for both IMF settings. The box shows the interquartile range and the whiskers present the full range of the metric scores. The median R exceeds 0.7 by three satellites, and rises to 0.75 by six satellites. Surpassing this 0.7 level is useful because this corresponds to coefficient of determination score (defined as R^2) of 0.5. R^2 is a measure of how much of the variance in one parameter is captured by similar variance in the other parameter (the two parameters, in this case, being the outflow fluxes). Therefore, a median R^2 of 0.5 indicates that 50% of the variance in the original outflow flux number sets is reproduced by the reconstructed number sets. To put it another way, passing an R of 0.7 means that the reconstructions contain a majority of the features in the original pattern.

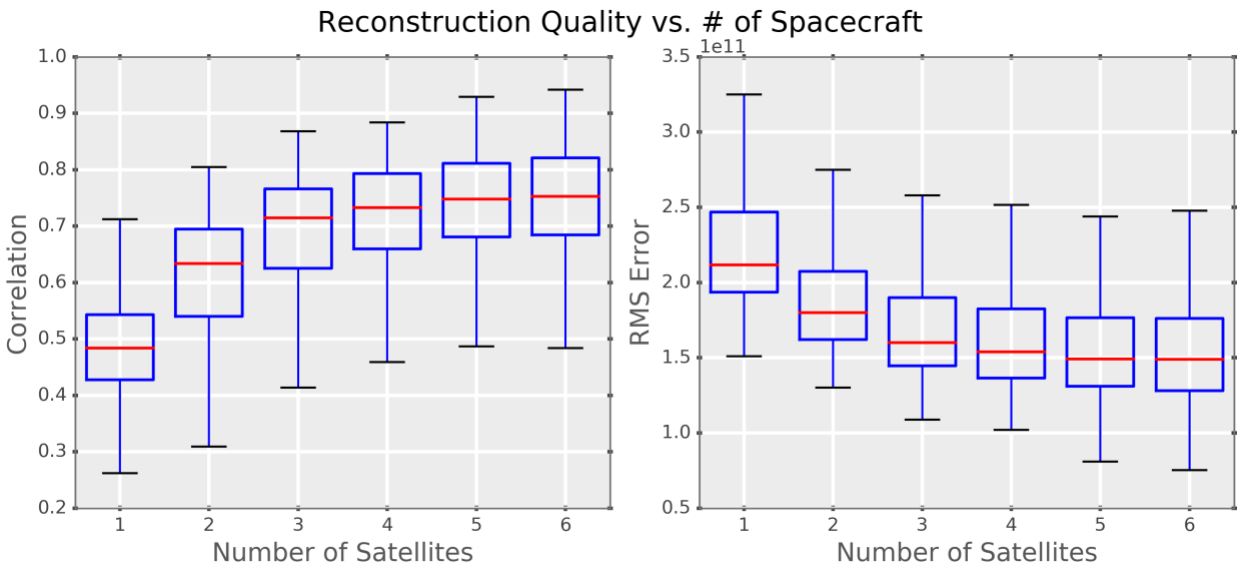

Figure 9. Correlation (R) and root mean square error (RMSE) as a function of the number of satellites used in the reconstruction. All reconstructions as a function of local time of orbit crossing, magnetic latitude of the crossing, nodal separation of the spacecraft, and geomagnetic activity are included. The red bar shows the median metric score, the box shows the interquartile range, and the whiskers extend to the extremes of the distributions.

There are two other features to note in Figure 10. The metrics medians appear to level off by three or four satellites in the constellation, and essentially asymptote at six satellites (i.e., no discernible no change from five satellites). The boxplot presentation also reveals asymmetries in the underlying histogram of values, showing a skew in all of the distributions with an elongated tail towards poorer reconstructions. This is because all of the parameter settings were included in the plot creation, including those with small satellite separation or badly aligned orbit plane crossing locations (relative to outflow features in the MHD patterns).

To investigate the spread in the boxplots of Figure 10, Figure 11 shows median RMSE scores and correlation coefficients as a function of two constellation parameters, the number of satellites and the magnetic latitude of the orbit plane crossing. Each white grid crossing in the plots is a constellation configuration setting for these two parameters, the color is smoothed to fill in each panel. All settings for the other two parameters are included in the number sets leading to the median values presented in Figure 11. Note that the colorscales for both of the metrics are optimized for the values in the plot and do not start at zero.

Magnetic latitude of the crossing is analogous to inclination of the orbit planes, but not the same, of course, because the magnetic poles are not aligned with the geographic poles, introducing a systematic diurnal variation to the magnetic latitude of the orbit crossing. That is, this is not a parameter of a real satellite mission, which would require weighted averaging of a span of magnetic latitude crossings to determine the accuracy for a given inclination. That said, this presentation is informative to help guide the choice of an optimal inclination for the constellation.

The clear feature of Figure 11 is that there is a peak in the metric scores (maximum R, minimum RMSE) at 80˚. Both metrics are noticeably worse for lower crossing latitudes; this is expected as the satellites spend little time in the auroral zone and therefore miss most of the outflow. The interesting result is that the metrics are worse for an 85˚ and 90˚ magnetic latitude crossing than for the optimal crossing of 80˚. This is because, at these high-inclination settings, the orbits are cutting through the auroral zone – where most of the outflow occurs – with a more

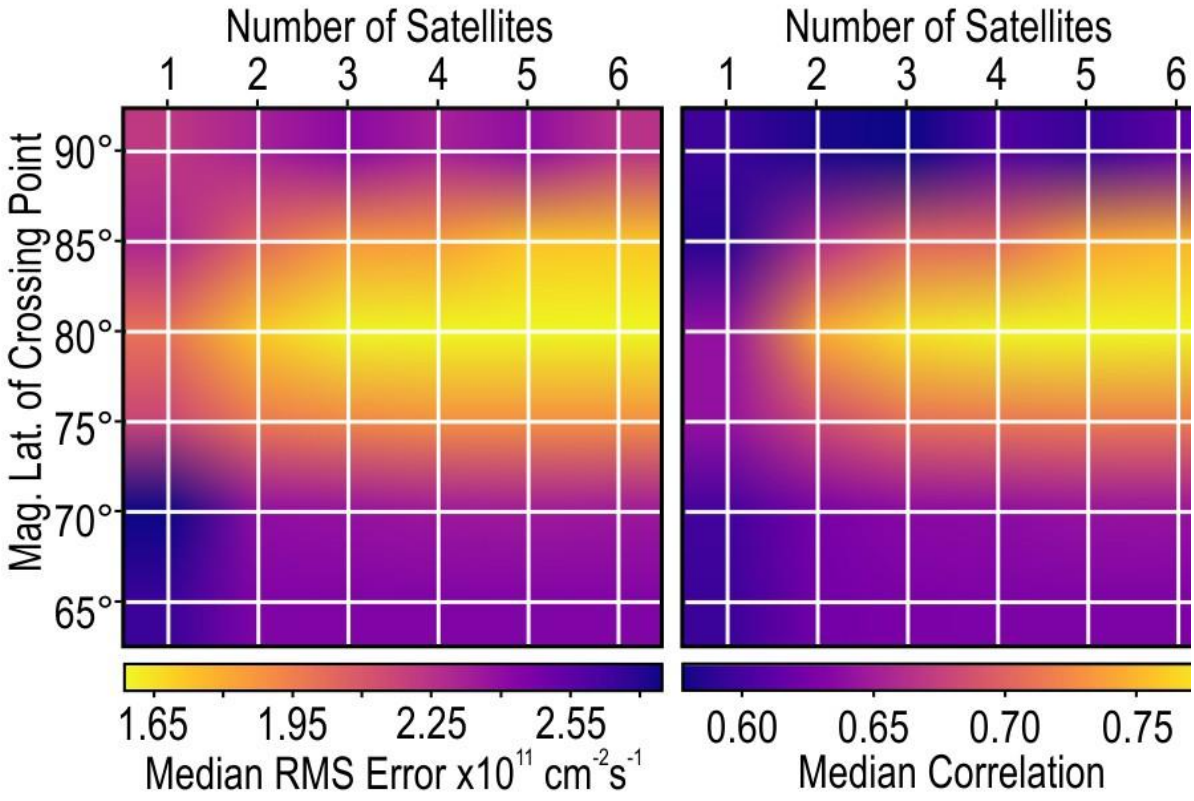

Figure 11. Metrics versus number of satellites and the magnetic latitude of the crossing point. The median metric is shown from the distribution of values from the remaining parameters in the reconstruction analysis.

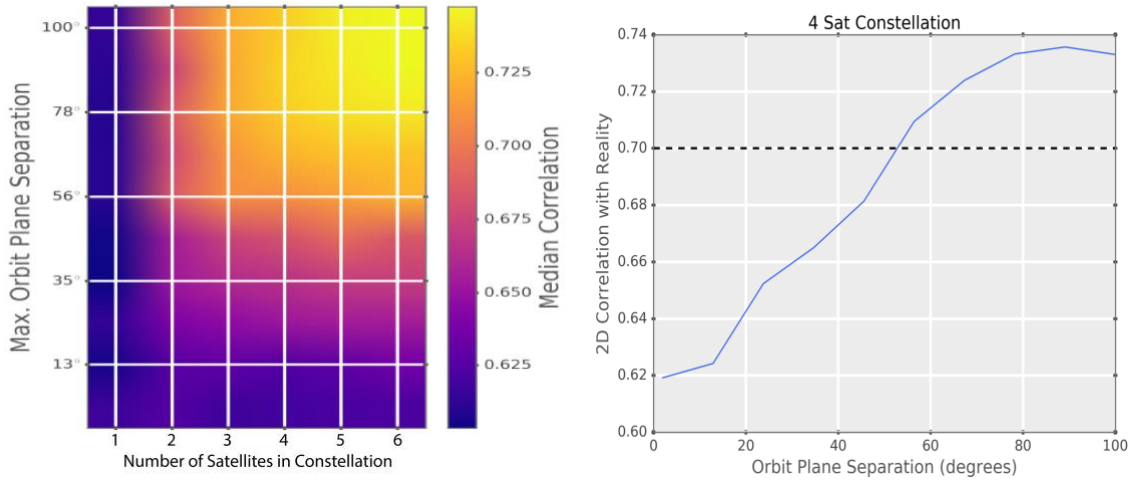

Figure 12. Left: Correlation coefficient as a function of number of spacecraft in the constellation (x axis) and the maximum orbit plan separation angle (y axis). The median score is shown from the distribution created by the other parameters in the analysis. Right: median correlation coefficient as a function of orbit plane separation for a four satellite constellation.

meridional trajectory. With a meridional trajectory, the satellites spend less time in the auroral zone and contribute fewer values to the reconstruction. There appears to be an optimal reconstruction for which the crossing is just poleward of the auroral zone, providing a maximal orbital path length through the entire latitude band of the high outflow flux.

Figure 12 shows median correlation coefficients as a function of the maximum orbit plane separation and number of satellites. Only correlation is shown here in order to present a different kind of second panel; the right plot is a slice through the other for the four-satellite constellation configuration. As with Figures 10 and 11, the RMSE results (not shown) reveal the same trends as the correlation plots included in the figure.

In Figure 12, it is seen that the best correlations are located in the upper right corner of the left panel. The reconstruction improves with both number of satellites and orbit plane separation. The right panel reveals a limit to this improvement, though, as the peak correlation is found at ~90˚ separation. As the maximum separation expands past 90˚, the inter-orbit separation of the constellation becomes large enough to start to miss meso-scale features (at least in some of the constellation configurations), and the median reconstruction slightly decreases. The drop in median correlation from 90˚ to 100˚ is not significant, but it is the start of a trend that will continue as the maximum orbit plane separation increases to 180˚. At that point, the two end

members of the constellation are flying along nearly the same trajectory but in opposite directions, therefore they are not contributing two satellites' worth of information to the reconstruction.

Also shown in the right panel of Figure 12 is that the median correlation coefficient for a 4-satellite constellation exceeds 0.7 for a maximum separation of 55˚ or more. This can be considered a cutoff threshold for producing reasonable reconstructions (in which most of the variation in the original pattern is captured by the reconstruction) with a reasonable number of satellites (four).

The magnetic local time of the orbit plane crossing did not show a trend in either RMSE or R. The spread is large and the differences in the median values were not significant and do not need to be shown. Parsing the study results further, this parameter only mattered for small orbit plane separation. For this case, very few of the reconstructions are of high quality, but a crossing on the nightside was marginally better than one on the dayside.

4.3. Outflow during a storm interval

The above analysis showed that 4 satellites with a >55˚ orbit plane separation between the end-member spacecraft produces fairly accurate reconstructions. That assessment, however, was conducted with only two outflow patterns, a nominal southward IMF case and a nominal northward IMF case, with standard solar wind parameters. It is useful to test the reconstruction method and the ability of a constellation to reconstruct outflow during a storm interval. Using the same SWMF model configuration as above, the "St. Patrick's Day Storm" of 17-18 March 2015 was simulated. For reference, the Dst time series for this storm is shown in the upper panel of Figure 13.

Outflow patterns were obtained from the SWMF every minute. Reconstructions were then compiled on a 2-hour cadence, which would be the cadence of a 2000 km altitude constellation presumably taking these outflow measurements. The number of spacecraft was set to four and the maximum orbit plane separation set to 90˚ (i.e., 30˚ separation between each of the orbit planes). To build up statistics, the local time and magnetic latitude of the crossing were varied, using four local times (00, 06, 12, and 18) and four latitudes (65˚, 75˚, 85˚, and 95˚). In all, 1920 reconstructions were conducted for each two-hour period throughout the storm interval.

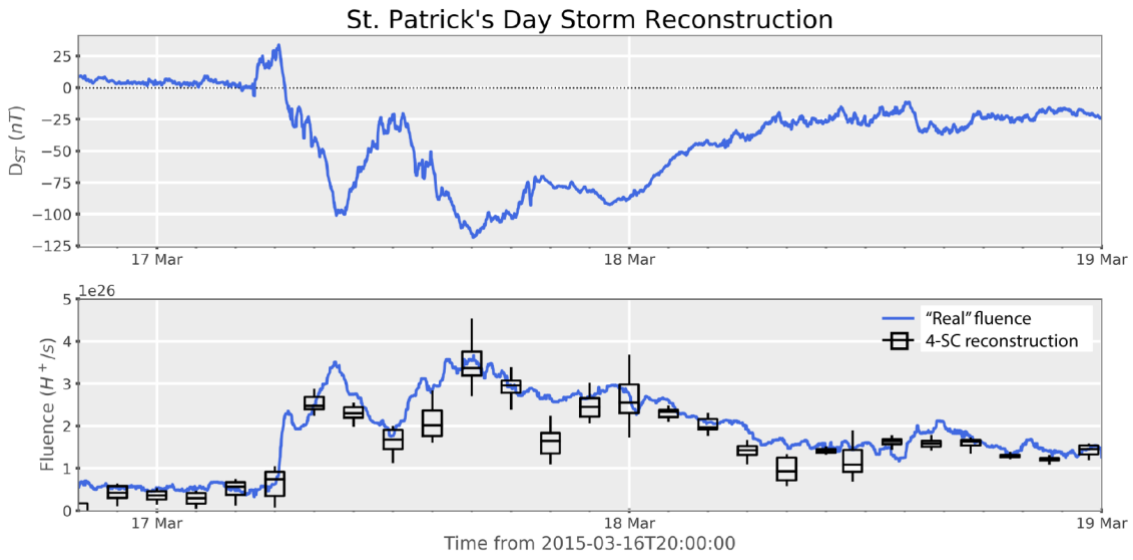

Figure 13. The top panel shows the Dst index time series during the 17-18 March 2015 magnetic storm interval. The bottom panel shows the northern hemisphere ionospheric outflow fluence from the MHD model (blue line) and the box-and-whisker distribution of fluences from the reconstructions.

To provide an overall assessment of the reconstructions, Figure 13 shows the time series of the integrated outflow fluence (lower panel), both from the SWMF model (on a one-minute cadence) and from the reconstructions (on a two-hour cadence as boxplots). Of the 26 boxplots in this figure, 19 have model values passing through the interquartile range of the reconstructed fluences (the "box" of the boxplot). The reconstructed fluences are usually at or below the original values, indicating that the reconstruction method usually captures the basic pattern of the outflow but not all of the meso-scale "hot spots" of elevated flux. There were a few times where the reconstructed fluences were entirely below the 120 original MHD fluences in that two-hour window, but for most of the intervals, the reconstructions are doing reasonably well.

5. Discussion on implementation

It is expected that a mission fulfilling the orbital requirements defined in section 4 above would consist of several identically-instrumented, longitudinally-separated, high-inclination spacecraft observing the low-energy ion velocity distribution above 1000 km altitude (in order to observe outflow, not upwelling) and below 3000 km altitude (to minimize orbital period and surface area of the orbit shell). Initial cost estimates suggest that such a mission could be

achieved within the constraints of the Heliophysics Small Explorer mission line with minimal instrumentation.

In its simplest configuration with only an ion spectrometer, this type of mission concept represents an important measurement paradigm that is ideally suited for the Explorer mission line. Instead of measuring "everything" at one or two locations, this constellation would "globally" measure one key plasma property. The satellites in the constellation would relate different portions of the high latitude ionospheric outflow with each other, connecting dayside with nightside outflow rates and revealing storm-sequence time lags and correlations. Significant progress in our understanding of ion outflow would be achieved with only the low-energy ion velocity space measurement at several locations, moving our understanding of system science of geospace as a whole to the next level. Note that if the full 4π field of view of the ion velocity distribution is measured by this ion instrument, then the downflowing low-energy ions would also be observed and subsequently constructed into maps every orbit period.

An alternative mission concept to the single instrument payload would be to design the spacecraft with additional instrumentation to provide observations that complement and contextualize the ion data. This would most likely need to be proposed at the Heliophysics Mid-sized Explorer level (or larger) to maintain the four-satellite constellation. With only one well-instrumented spacecraft, the mission would repeat the findings of the FAST or Akebono missions and would not be particularly innovative without some other major design augmentation to make it worthy of the investment.

A limitation of this study is that it is assumed that the outflow pattern is steady for the duration of the high-latitude passage of the constellation, i.e., 20 to 30 minutes. This is a somewhat reasonable assumption, given that the outflowing ions are moving at only a few to tens of kilometers per second, and therefore take many minutes to flow from the ionosphere (let's say the starting altitude is in the topside ionosphere at 300 km altitude) to a nominal observation altitude of around 2000 km. If an ion is accelerated along the field line with just enough force to barely overcome gravity and maintain a 1 km/s upward velocity, then it would take 28 minutes for this ion to traverse this 1700 km distance and reach the satellite. If, however, the outflowing ions maintain a velocity of 10 km/s, then this trip would only take 3 minutes. Furthermore, the outflow pattern can only be constructed once per orbit (per hemisphere), so the cadence of the

patterns would be on the order of 2 hours. This mission concept, therefore, is not suitable for investigating prompt outflow events, but rather for the investigation of longer-term outflow and its consequences on the magnetosphere. If proposed to the Heliophysics Mid-sized Explorer program, or if a very inexpensive miniaturized ion instrument is used, then a fleet of small satellites could be deployed with several along each of the four orbit planes, allowing for a faster cadence of the reconstructed outflow patterns.

6. Conclusion

This study addressed the question of how many satellites would be needed to accurately reconstruct the high-latitude ionospheric outflow pattern. An observing system simulation experiment was conducted to quantify and constrain the requirements for a reasonable reconstruction of the outflow pattern. With "accurate" defined as a median correlation coefficient of 0.7 for a sensitivity study spanning several orbital configuration parameters and IMF settings, the answer is four. Three might work, but one or two satellites is inadequate for the task. Five or six satellites produce slightly better reconstructions, but the marginal improvement might not be worth the cost unless the focus is on the meso-scale features of ionospheric outflow. It is best to maximize auroral zone dwell time for the constellation, so an inclination between 75˚ and 85˚ is best. Higher than this and the orbit planes would cut too quickly through the high outflow flux region, and lower than this and they would likely miss the outflow regions on many passes. The orbit planes should spread across a wide swath of local times, with a separation between the end-member spacecraft of at least 60˚, and 90˚ would be even better. More than this separation produces marginal improvement or even diminished accuracy. The local time of the orbital plane crossings was not significant in controlling the accuracy of the reconstructed outflow pattern.

This study provides a starting point for future mission concept development on measuring the global pattern of ionospheric outflow. Because of the heavy mass of O^+, N^+ and other constituents in this outflow, understanding the full high-latitude spatial structure and temporal variability of the escaping ions is vital for scientific progress on the ionosphere-magnetosphere relationship and nonlinear feedback loop. Ionospheric outflow mass loads the magnetosphere and significantly impacts many physical processes, to the point of reshaping the magnetosphere and altering the large-scale dynamics of near-Earth space. This is a critical unresolved question in space physics and a dedicated mission would substantially advance our community's

understanding of geospace system dynamics and space weather predictions. This proposed mission would reveal the temporal change in ionospheric outflow on the timescales of substorm and storm phases and the relationship of this change to solar wind and IMF driving conditions. It would resolve both small scale outflows (early mission) and global outflow conditions (mid- to late-phase). Spatial outflow maps will be created every orbit, providing continuous coverage across storms. These observations would unlock the dynamic relationship between ionospheric outflow, solar wind drivers, and geomagnetic activity.

Acknowledgments and Data

The authors thank the University of Michigan and Southwest Research Institute for support of this project. The authors would like to thank the University of Michigan for its financial support, Southwest Research Institute for its financial support, and the US government, in particular research grants from NASA (specifically, grant numbers 80NSSC19K0077, 80NSSC21K1127, and 80NSSC21K1405) and NSF (specifically, grant AGS-1414517). MB was supported by the Office of Naval Research. All authors listed have made a substantial, direct, and intellectual contribution to the work and approved it for publication. The simulations were conducted by DTW and analyzed by DTW and MWL. An undergraduate student, Joshua Adam, also contributed to the plots and calculations. The datasets generated and analyzed for this study can be found in the University of Michigan Deep Blue DataSets repository [DOI LINK TBD upon manuscript acceptance and finalization].

References

Abe, T., B.A. Whalen, A.W. Yau, S. Watanabe, E. Sagawa, and K.I. Oyama (1993). Altitude profile of the polar wind velocity and its relationship to ionospheric conditions, Geophys. Res. Lett. (ISSN 0094-8276), 20 (24), 2825–2828.

Abe, T., A.W. Yau, S. Watanabe, M. Yamada, and E. Sagawa (2004). Long-term variation of the polar wind velocity and its implication for the ion acceleration process: Akebono/suprathermal ion mass spectrometer observations, J. Geophys. Res., 109 (A9), A09,305, doi: 10.1029/2003JA010223.

André, M., and A. Yau (1997). Theories and Observations of Ion Energization and Outflow in the High Latitude Magnetosphere, Space Science Reviews, 80 (1), 27–48.

André, M., K. Li, and A.I. Eriksson (2015). Outflow of low-energy ions and the solar cycle, J. Geophys. Res.: Space Physics, doi:10.1002/2014JA020714.

669 Banks, P. M., & Holzer, T. E. (1968). The polar wind. *Journal of Geophysical Research*, *73*(21),
670 6846-6854.

671 Barakat, A. R., Demars, H. G., & Schunk, R. W. (1998). Dynamic features of the polar wind in
672 the presence of hot magnetospheric electrons. *Journal of Geophysical Research: Space*
673 *Physics*, *103*(A12), 29289-29303.

674 Brambles, O.J., W. Lotko, P.A. Damiano, B. Zhang, M. Wiltberger, and J. Lyon (2010). Effects
675 of causally driven cusp O+ outflow on the storm time magnetosphere-ionosphere system
676 using a multifluid global simulation, J. Geophys. Res., 115, A00J04,
677 doi:10.1029/2010JA015469.

678 Brambles, O.J., W. Lotko, B. Zhang, M. Wiltberger, J. Lyon, and R.J. Strangeway (2011).
679 Magnetosphere sawtooth oscillations induced by ionospheric outflow, Science, 332
680 (6034), 1183–6, doi:10.1126/science.1202869.

681 Brambles, O.J., W. Lotko, B. Zhang, J. Ouellette, J. Lyon, and M. Wiltberger (2013). The effects
682 of ionospheric outflow on ICME and SIR driven sawtooth events, J. Geophys. Res.:
683 Space Physics, 118 (10), 6026–6041, doi:10.1002/jgra.50522.

684 Brinton, H.C., J.M. Grebowsky, and H.G. Mayr (1971). Altitude Variation of Ion Composition in
685 Midlatitude Trough Region - Evidence for Upward Plasma Flow, J. Geophys. Res.: Space
686 Physics, 76 (16), 3738–&.

687 Chandler, M.O., T.E. Moore, and J.H. Waite (1991). Observations of polar ion outflows, J.
688 Geophys. Res. (ISSN 0148-0227), 96 (A2), 1421–1428.

689 Chappell, C.R. (2015). The Role of the Ionosphere in Providing Plasma to the Terrestrial
690 Magnetosphere: An Historical Overview, Space Science Reviews, 192 (1-4), 5–25,
691 doi:10.1007/s11214-015-0168-5.

692 Chappell, C.R., T.E. Moore, and J.H. Waite, Jr. (1987). The ionosphere as a fully adequate
693 source of plasma for the earth's magnetosphere, J. Geophys. Res., 92, 5896–5910, doi:
694 10.1029/JA092iA06p05896.

695 Chappell, C. R., R. C. Olsen, J. L. Green, J.F.E. Johnson, and J. H. Waite, Jr. (1982). The
696 discovery of nitrogen ions in the earth's magnetosphere, Geophys. Res. Lett., 9, 937-940.

697 Chaston, C. C., Bonnell, J. W., Reeves, G. D., & Skoug, R. M. (2016). Driving ionospheric
698 outflows and magnetospheric O^+ energy density with Alfvén waves. *Geophysical*
699 *Research Letters*, *43*(10), 4825-4833.

700 Christon, S. P., *et al. (2000).* Low charge state heavy ions upstream of Earth's bow shock and
701 sunward flux of ionospheric O^{+1}, N^{+1}, and O^{+2} ions: Geotail observations, *Geophys. Res.*
702 *Lett.*, *27*, 2433–2436.

703 Christon, S.P., U. Mall, T.E. Eastman, G. Gloeckler, A.T.Y. Lui, R.W. McEntire, and E.C.
704 Roelof (2002). Solar cycle and geomagnetic N^{+1}/O^{+1} variation in outer dayside
705 magnetosphere: Possible relation to topside ionosphere, Geophys. Res. Lett., 29 (5), 2–1–
706 2–3.

707 Cladis, J. B. (1986). Parallel acceleration and transport of ions from polar ionosphere to plasma
708 sheet. *Geophysical Research Letters*, *13*(9), 893-896.

Coley, W.R., R.A. Heelis, and M.R. Hairston (2003). High-latitude plasma outflow as measured by the DMSP spacecraft, J. Geophys. Res., 108(A), 1441.

Cully, C.M., E. Donovan, A.W. Yau, and G.G. Arkos (2003). Akebono/Suprathermal Mass Spectrometer observations of low-energy ion outflow: Dependence on magnetic activity and solar wind conditions, J. Geophys. Res., 108 (A2), 1093, doi:10.1029/2001JA009200.

Daglis, I.A., R.M. Thorne, W. Baumjohann, and S. Orsini (1999). The terrestrial ring current: Origin, formation, and decay, Reviews of Geophysics, 37, 407–438, doi:10.1029/1999RG900009.

Dandouras, I. (2021). Ion outflow and escape in the terrestrial magnetosphere: Cluster advances. *Journal of Geophysical Research: Space Physics*, *126*(10), e2021JA029753, doi: 10.1029/2021JA029753

Delcourt, D.C., C.R. Chappell, T.E. Moore, and J.H. Waite (1989). A three-dimensional numerical model of ionospheric plasma in the magnetosphere, J. Geophys. Res., 94 (A9), 11,893,doi:10.1029/JA094iA09p11893.

Delcourt, D.C., J.A. Sauvaud, and T.E. Moore (1993). Polar wind ion dynamics in the magnetotail, J. Geophys. Res., 98 (A6), 9155, doi:10.1029/93JA00301.

Demars, H. G., Barakat, A. R., & Schunk, R. W. (1996). Effect of centrifugal acceleration on the polar wind. *Journal of Geophysical Research: Space Physics*, *101*(A11), 24565-24571.

Denton, M.H., M.F. Thomsen, H. Korth, S. Lynch, J.C. Zhang, and M.W. Liemohn (2005). Bulk plasma properties at geosynchronous orbit, J. Geophys. Res.: Space Physics, 110 (A9), 7223–+, doi:10.1029/2004JA010861.

Elliott, H.A., R.H. Comfort, P.D. Craven, M.O. Chandler, and T.E. Moore (2001). Solar wind influence on the oxygen content of ion outflow in the high-altitude polar cap during solar minimum conditions, J. Geophys. Res., 106 (A4), 6067, doi:10.1029/2000JA003022.

Elliott, H. A., Jahn, J. M., Pollock, C. J., Moore, T. E., & Horwitz, J. L. (2007). O^+ transport across the polar cap. *Journal of atmospheric and solar-terrestrial physics*, *69*(13), 1541-1555.

Engwall, E., A.I. Eriksson, C.M. Cully, M. Andre, P.A. Puhl-Quinn, H. Vaith, and R. Torbert (2009). Survey of cold ionospheric outflows in the magnetotail, Annales Geophysicae, 27(8), 3185–3201, doi:10.5194/angeo-27-3185-2009.

Farrell, W.M., and J.A. Van Allen (1990). Observations of the Earth's polar cleft at large radial distances with the Hawkeye 1 Magnetometer, J. Geophys. Res., 95 (A12), 20,945, doi: 10.1029/JA095iA12p20945.

Foster, J. C., St.-Maurice, J. P., & Abreu, V. J. (1983). Joule heating at high latitudes. *Journal of Geophysical Research: Space Physics*, *88*(A6), 4885-4897.

Fritsch, F. N., & Carlson, R. E. (1980). Monotone piecewise cubic interpolation. *SIAM Journal on Numerical Analysis*, *17*(2), 238-246.

747 Fung, S.,T. Eastman, S. Boardsen, and S.-H. Chen (1997). High-altitude cusp positions sampled
748 by the Hawkeye satellite, Physics and Chemistry of the Earth, 22 (7-8), 653–662, doi:
749 10.1016/S0079-1946(97)88121-9.

750 Fuselier, S. A., Mende, S. B., Moore, T. E., Frey, H. U., Petrinec, S. M., Claflin, E. S., & Collier,
751 M. R. (2003). Cusp dynamics and ionospheric outflow. *Magnetospheric Imaging—The*
752 *Image Prime Mission*, 285-312.

753 Ganguli, S. B. (1996), The polar wind, *Rev. Geophys.*, 34(3), 311– 348,
754 doi:10.1029/96RG00497.

755 Garcia, K.S., V.G. Merkin, and W.J. Hughes (2010). Effects of nightside O^+ outflow on
756 magnetospheric dynamics: Results of multifluid MHD modeling, J. Geophys. Res.: Space
757 Physics, 115, A00J09, doi:10.1029/2010JA015730.

758 Giles, B.L., C.R. Chappell, T.E. Moore, R.H. Comfort, and J.H. Waite (1994). Statistical survey
759 of pitch angle distributions in core (0-50 eV) ions from Dynamics Explorer, 1: Outflow in
760 the auroral zone, polar cap, and cusp, J. Geophys. Res., 99 (A9), 17,483,
761 doi:10.1029/94JA00864.

762 Glocer, A., & Daldorff, L. K. S. (2022). Connecting energy input with ionospheric upflow and
763 outflow. *Journal of Geophysical Research: Space Physics*, 127,
764 e2022JA030635. https://doi.org/10.1029/2022JA030635

765 Glocer, A., G. Toth, T. Gombosi, and D. Welling (2009a). Modeling ionospheric outflows and
766 their impact on the magnetosphere, initial results, J. Geophys. Res.: Space Physics, 114
767 (A13), 5216–+, doi:10.1029/2009JA014053.

768 Glocer, A., G. Toth, Y. Ma, T. Gombosi, J.-C. Zhang, and L.M. Kistler (2009b). Multifluid
769 Block-Adaptive-Tree Solar wind Roe-type Upwind Scheme: Magnetospheric
770 composition and dynamics during geomagnetic storms: Initial results, J. Geophys. Res.:
771 Space Physics, 114(A13), A12203, doi:10.1029/2009JA014418.

772 Glocer, A., N. Kitamura, G. Toth, and T. Gombosi (2012). Modeling solar zenith angle effects
773 on the polar wind, J. Geophys. Res.: Space Physics, 117 (A16), A04318, doi:
774 10.1029/2011JA017136.

775 Glocer, A., G. V. Khazanov, and M. W. Liemohn (2017), Photoelectrons in the quiet polar wind,
776 *J. Geophys. Res. Space Physics*, *122*, 6708-6726, doi: 10.1002/2017JA024177.

777 Glocer, A., Toth, G., & Fok, M.-C. (2018). Including kinetic ion effects in the coupled global
778 ionospheric outflow solution. *Journal of Geophysical Research: Space*
779 *Physics*, *123*, 2851–2871. https://doi.org/10.1002/2018JA025241

780 Gloeckler, G., F.M. Ipavich, B. Wilken, W. Stuedemann, and D. Hovestadt (1985). First
781 composition measurement of the bulk of the storm-time ring current (1 to 300 keV/e)
782 with AMPTE-CCE, Geophys. Res. Lett., 12, 325–328, doi:10.1029/GL012i005p00325.

783 Gombosi, T. I., & Killeen, T. L. (1987). Effects of thermospheric motions on the polar wind: A
784 time-dependent numerical study. *Journal of Geophysical Research: Space Physics*,
785 *92*(A5), 4725-4729.

786 Gombosi, T. I., Chen, Y., Glocer, A., Huang, Z., Liemohn, M. W., Manchester, W. B.,
787 Pulkkinen, T., Schdeva, N., Shidi, Q., Sokolov, I. V., Szente, J., Tenishev, V., Toth, G.,

van der Holst, B., Welling, D. T., Zhao, L., & Zou, S. (2021). What sustained multi-disciplinary research can achieve: The Space Weather Modeling Framework. *Journal of Space Weather and Space Climate*, *11*, 42. https://doi.org/10.1051/swsc/2021020

Gurgiolo, C., & Burch, J. L. (1982). DE-1 observations of the polar wind—A heated and an unheated component. *Geophysical Research Letters*, *9*(9), 945-948.

Hamilton, D.C., G. Gloeckler, F.M. Ipavich, B. Wilken, and W. Stuedemann (1988). Ring current development during the great geomagnetic storm of February 1986, J. Geophys. Res., 93, 14,343–14,355,doi:10.1029/JA093iA12p14343.

Hoffman, J.H., and W.H. Dodson (1980). Light ion concentrations and fluxes in the polar regions during magnetically quiet times, J. Geophys. Res., 85(A2), 626–632.

Horwitz, J. L., Ho, C. W., Scarbro, H. D., Wilson, G. R., & Moore, T. E. (1994). Centrifugal acceleration of the polar wind. *Journal of Geophysical Research: Space Physics*, *99*(A8), 15051-15064.

Huddleston, M.M., C.R. Chappell, D.C. Delcourt, T.E. Moore, B.L. Giles, and M.O. Chandler (2005). An examination of the process and magnitude of ionospheric plasma supply to the magnetosphere, J. Geophys. Res.: Space Physics, 110 (A9), A12202, doi:10.1029/2004JA010401.

Hultqvist, B., André, M., Christon, S. *et al.* (1999). Contributions of different source and loss processes to the plasma content of the magnetosphere. *Space Science Reviews* **88**, 355–372. https://doi.org/10.1023/A:1005260002333

Ilie, R., and M. W. Liemohn (2016), The outflow of ionospheric nitrogen ions: a possible tracer for the altitude dependent transport and energization processes of ionospheric plasma, *J. Geophys. Res. Space Physics*, *121*, 9250-9255, doi: 10.1002/2015JA022162.

Ilie, R., R.M. Skoug, P. Valek, H.O. Funsten, and A. Glocer (2013). Global view of inner magnetosphere composition during storm time, J. Geophys. Res.: Space Physics, 118 (1), 7074–7084.

Ilie, R., M.W. Liemohn, G. Toth, N. Yu Ganushkina, and L.K.S. Daldorff (2015). Assessing the role of oxygen on ring current formation and evolution through numerical experiments, J. Geophys. Res.: Space Physics, 120 (6), 4656–4668, doi:10.1002/2015JA021157, 2015JA021157.

Khazanov, G. V., M. W. Liemohn, and T. E. Moore (1997). Photoelectron effects on the self-consistent potential in the collisionless polar wind, *J. Geophys. Res.*, *102*, 7509.

Kistler, L.M., et al. (2006). Ion composition and pressure changes in storm time and nonstorm substorms in the vicinity of the near-Earth neutral line, J. Geophys. Res.: Space Physics, 111(A), A11,222.

Kistler, L.M., C.G. Mouikis, B. Klecker, and I. Dandouras (2010a). Cusp as a source for oxygen in the plasma sheet during geomagnetic storms, J. Geophys. Res., 115 (A3), A03,209, doi:10.1029/2009JA014838.

Kistler, L.M., et al. (2010b). Escape of O^+ through the distant tail plasma sheet, Geophys. Res. Lett., 37(21), doi:10.1029/2010GL045075.

Kistler, L.M., et al. (2010c). Escape of O^+ through the distant tail plasma sheet, Geophys. Res. Lett., 37(2), L21,101.

Kistler, L.M., et al. (2016). The source of O^+ in the storm time ring current, J. Geophys. Res.: Space Physics, 121 (6), 5333–5349, doi:10.1002/2015JA022204, 2015JA022204.

Kitamura, N., et al. (2010). Observations of very-low-energy (<10 eV) ion outflows dominated by O^+ ions in the region of enhanced electron density in the polar cap magnetosphere during geomagnetic storms, J. Geophys. Res., 115, A00J06, doi:10.1029/2010JA015601.

Kronberg, E.A., S.E. Haaland, P.W. Daly, E.E. Grigorenko, L.M. Kistler, M. Fränz, and I. Dandouras (2012). Oxygen and hydrogen ion abundance in the near-Earth magnetosphere: Statistical results on the response to the geomagnetic and solar wind activity conditions, J. Geophys. Res., 117 (A12), A12,208, doi:10.1029/2012JA018071.

Kronberg, E.A., et al. (2014). Circulation of Heavy Ions and Their Dynamical Effects in the Magnetosphere: Recent Observations and Models, Space Science Reviews, 184 (1-4), 173-235, doi: 10.1007/s11214-014-0104-0.

Lemaire, J. (1971). Effect of escaping photoelectrons in a polar exospheric model.

Lennartsson, O.W. (1995). Statistical investigation of IMF Bz effects on energetic (0.1- to 16-keV) magnetospheric O^+ ions J. Geophys. Res., 100 (A), 23,621–23,636.

Lennartsson, W., and E.G. Shelley (1986). Survey of 0.1- to 16-keV/e plasma sheet ion composition, J. Geophys. Res.: Space Physics (1978–2012), 91 (A3), 3061–3076.

Lennartsson, O. W., Collin, H. L., and Peterson, W. K. (2004), Solar wind control of Earth's H^+ and O^+ outflow rates in the 15-eV to 33-keV energy range, *J. Geophys. Res.*, 109, A12212, doi:10.1029/2004JA010690.

Liao, J., L.M. Kistler, C.G. Mouikis, B. Klecker, I. Dandouras, and J.-C. Zhang (2010). Statistical study of O^+ transport from the cusp to the lobes with Cluster CODIF data, J. Geophys. Res., 115(September),A00J15, doi:10.1029/2010JA015613.

Liao, J., Kistler, L. M., Mouikis, C. G., Klecker, B., & Dandouras, I. (2015). Acceleration of O+ from the cusp to the plasma sheet. *Journal of Geophysical Research: Space Physics*, *120*(2), 1022-1034.

Liemohn, M. W., T. E. Moore, P. D. Craven, W. Maddox, A. F. Nagy, and J. U. Kozyra (2005). Occurrence statistics of cold, streaming ions in the near-Earth magnetotail: Survey of Polar-TIDE observations, *J. Geophys. Res., 110,* A07211, doi: 10.1029/2004JA010801.

Liemohn, M. W., T. E. Moore, and P. D. Craven (2007). Geospace activity dependence of cold, streaming ions in the near-Earth magnetotail, *J. Atmos. Solar-Terr. Phys., 69*, 135.

Liemohn, M. W., and D. T. Welling (2016), Ionospheric and solar wind contributions to magnetospheric ion density and temperature throughout the magnetotail, in *Magnetosphere-Ionosphere Coupling in the Solar System, Geophys. Monogr. Ser., vol. 222*, edited by C. R. Chappell, R. Schunk, P. Banks, J. Burch, and R. Thorne, John Wiley and Sons, Inc., Hoboken, NJ, USA, doi: 10.1002/9781119066880.ch8, 101-114.

Liemohn, M. W., Shane, A. D., Azari, A. R., Petersen, A. K., Swiger, B. M., & Mukhopadhyay, A. (2021). RMSE is not enough: guidelines to robust data-model comparisons for

magnetospheric physics. *Journal of Atmospheric and Solar-Terrestrial Physics*, *218*, 105624. https://doi.org/10.1016/j.jastp.2021.105624

Liemohn, M. W., Jörg-Micha Jahn, Raluca Ilie, Natalia Ganushkina, and Daniel Welling (2022). Science case for a global ionospheric outflow mission. White paper to the Decadal Survey for Solar and Space Physics 2024-2033. Paper # 409.

Lin M-Y and Ilie R (2022). A Review of Observations of Molecular Ions in the Earth's Magnetosphere-Ionosphere System. Front. Astron. Space Sci. 8:745357. doi: 10.3389/fspas.2021.745357

Lin. M. Y., R. Ilie, and A. Glocer (2020), The Contribution of N^+ ions to Earth's Polar Wind. Geophysical Research Letters, 47, https://doi.org/10.1029/2020GL089321

Liu, C., Horwitz, J. L., & Richards, P. G. (1995). Effects of frictional ion heating and soft-electron precipitation on high-latitude F-region upflows. *Geophysical Research Letters*, *22*(20), 2713-2716.

Liu, W.L., S.Y. Fu, Q.G. Zong, Z.Y. Pu, J. Yang, and P. Ruan (2005). Variations of N^+/O^+ in the ring current during magnetic storms, Geophys. Res. Lett., 32(1), L15,102.

Lockwood, M., M.F. Smith, C.J. Farrugia, and G.L. Siscoe (1988). Ionospheric ion upwelling in the wake of flux transfer events at the dayside magnetopause, J. Geophys. Res. (ISSN 0148-0227), 93 (A6), 5641–5654.

Lund, E. J., Nowrouzi, N., Kistler, L. M., Cai, X., & Frey, H. U. (2018). On the role of ionospheric ions in sawtooth events. *Journal of Geophysical Research: Space Physics*, 123, 665– 684. https://doi.org/10.1002/2017JA024378

Lundin, R., & Guglielmi, A. (2006). Ponderomotive forces in cosmos. *Space Science Reviews*, *127*, 1-116.

Lui, A. T. Y., and Hamilton, D. C. (1992), Radial profiles of quiet time magnetospheric parameters, *J. Geophys. Res.*, 97(A12), 19325–19332, doi:10.1029/92JA01539.

Lynch, K. A., Semeter, J. L., Zettergren, M., Kintner, P., Arnoldy, R., Klatt, E., ... & Samara, M. (2007). Auroral ion outflow: Low altitude energization. In *Annales Geophysicae* (Vol. 25, No. 9, pp. 1967-1977). Göttingen, Germany: Copernicus Publications.

Mall, U., S. Christon, E. Kirsch, and G. Gloeckler (2002). On the solar cycle dependence of the N^+/O^+ content in the magnetosphere and its relation to atomic N and O in the Earth's exosphere, Geophys. Res. Lett., 29 (1), 1593–34–3.

Miller, R. H., Rasmussen, C. E., Combi, M. R., Gombosi, T. I., & Winske, D. (1995). Ponderomotive acceleration in the auroral region: A kinetic simulation. *Journal of Geophysical Research: Space Physics*, *100*(A12), 23901-23916.

Moore, T. E. (1984). Superthermal ionospheric outflows. *Reviews of Geophysics*, *22*(3), 264-274.

Moore, T. E., & Delcourt, D. C. (1995). The geopause. *Reviews of Geophysics*, *33*(2), 175–209. https://doi.org/10.1029/95RG00872

Moore, T. E., and Horwitz, J. L. (2007), Stellar ablation of planetary atmospheres, *Rev. Geophys.*, 45, RG3002, doi:10.1029/2005RG000194.

Moore, T.E., Chappell, C.R., Chandler, M.O., Fields, S.A., Pollock, C.J., Reasoner, D.L., Young, D.T., Burch, J.L., Eaker, N., Waite Jr., J.H., McComas, D.J., Nordholdt, J.E., Thomsen, M.F., Berthelier, J.J., Robson, R., Mozer, F.S. (1997). High altitude observations of the polar wind. Science, 277, 349–351.

Moore, T.E., et al. (1999a). Ionospheric mass ejection in response to a CME, Geophys. Res. Lett., 26 (1), 2339–2342.

Moore, T. E., Chandler, M. O., Chappell, C. R., Comfort, R. H., Craven, P. D., Delcourt, D. C., ... & Su, Y. J. (1999b). Polar/TIDE results on polar ion outflows. *Geophysical Monograph-American Geophysical Union*, *109*, 87-102.

Moore, T. E., M.-C. Fok, M. O. Chandler, S.-H. Chen, S. P. Christon, D. C. Delcourt, J. Fedder, M. Liemohn, W. K. Peterson, and S. Slinker (2005a). Solar and ionospheric plasmas in the ring current, *Inner Magnetosphere Interactions: New Perspectives from Imaging, AGU Monogr. Ser.*, vol. 159, ed. by J. L. Burch, M. Schulz, and H. Spence, p. 179, Am. Geophys. Un., Washington, D. C..

Moore, T. E., M.-C. Fok, M. O. Chandler, C. R. Chappell, S. Christon, D. Delcourt, J. Fedder, M. Huddleston, M. Liemohn, W. Peterson, S. P. Slinker (2005b). Plasma sheet and (non-storm) ring current formation from solar and polar wind sources, *J. Geophys. Res., 110*, A02210, doi: 10.1029/2004JA010563.

Moore, T., M.-C. Fok, and K. Garcia-Sage (2014). The ionospheric outflow feedback loop, Journal of Atmospheric and Solar-Terrestrial Physics, 115-116, 59–66, doi:10.1016/j.jastp.2014.02.002.

Mouikis, C.G., L.M. Kistler, Y.H. Liu, B. Klecker, A. Korth, and I. Dandouras (2010). H^+ and O^+ content of the plasma sheet at 15-19 Re as a function of geomagnetic and solar activity, J. Geophys. Res.: Space Physics, 115, A00J16, doi:10.1029/2010JA015978.

Nagai, T., J.H. Waite, J.L. Green, C.R. Chappell, R.C. Olsen, and R.H. Comfort (1984). First measurements of supersonic polar wind in the polar magnetosphere, Geophys. Res. Lett., 11 (7), 669–672.

Newell, P.T., and C.-I. Meng (1994). Ionospheric projections of magnetospheric regions under low and high solar wind pressure conditions, J. Geophys. Res., 99 (A1), 273, doi: 10.1029/93JA02273.

Nilsson, H., Kirkwood, S., Eliasson, L., Norberg, O., Clemmons, J., & Boehm, M. (1994). The ionospheric signature of the cusp: A case study using Freja and the Sondrestrom radar. *Geophysical research letters*, *21*(17), 1923-1926.

Nosé, M., R.W. McEntire, and S.P. Christon (2003). Change of the plasma sheet ion composition during magnetic storm development observed by the Geotail spacecraft, J. Geophys. Res.: Space Physics, 108 (A), 1201.

Nosé, M., S. Taguchi, K. Hosokawa, S.P. Christon, R.W. McEntire, T.E. Moore, and M.R. Collier (2005). Overwhelming O^+ contribution to the plasma sheet energy density during the October 2003 superstorm: Geotail/EPIC and IMAGE/LENA observations. Journal of Geophysical Research Space Physics, 110 (A).

948 Øieroset, M., M. Yamauchi, L. Liszka, S.P. Christon, and B. Hultqvist (1999). A statistical study
949 of ion beams and conics from the dayside ionosphere during different phases of a
950 substorm, J. Geophys. Res.: Space Physics, 104 (A4), 6987–6998, doi:10.1029/
951 1998JA900177.

952 Ogawa, Y., S.C. Buchert, R. Fujii, S. Nozawa, and A.P. van Eyken (2009). Characteristics of ion
953 upflow and downflow observed with the European Incoherent Scatter Svalbard radar, J.
954 Geophys. Res.,, 114 (A), A05,305–n/a.

955 Peroomian, V., El-Alaoui, M., Ashour Abdalla, M., & Zelenyi, L. (2006). A comparison of solar
956 wind and ionospheric plasma contributions to the September 24-25, 1998 magnetic
957 storm. Journal of Atmospheric and Solar-Terrestrial Physics, 69, 212-222.
958 https://doi.org/10.1016/j.jastp.2006.07.025

959 Peterson, W.K., H.L. Collin, O.W. Lennartsson, and A.W. Yau, Quiet time solar illumination
960 effects on the fluxes and characteristic energies of ionospheric outflow, J. Geophys. Res.:
961 Space Physics, 111 (A), A11S05, 2006.

962 Pitout, F., C.P. Escoubet, B. Klecker, and H. R`eme, Cluster survey of the mid-altitude cusp: 1.
963 size, location, and dynamics, Annales Geophysicae, 24 (11), 3011–3026, doi:10.5194/
964 angeo-24-3011-2006, 2006.

965 Pollock, C. J., M. O. Chandler, T. E. Moore, J. H. Waite Jr., C. R. Chappell and D. A. Gurnett
966 (1990). A Survey of Upwelling Ion Event Characteristics, J. Geophys. Res. 95, 18969.

967 Pulkkinen, T. I., N. Yu. Ganushkina, D. N. Baker, N. E. Turner, J. Fennell, J. Roeder, T. A. Fritz,
968 M. Grande, B. Kellett, G. Kettmann (2001). Ring current ion composition during solar
969 minimum and rising solar activity: Polar/CAMMICE/MICS results, *Journal of*
970 *Geophysical Research, 106,* 19131-19147.

971 Rastätter, L., et al. (2013), Geospace environment modeling 2008–2009 challenge: D_{st} index,
972 *Space Weather*, 11, 187– 205, doi:10.1002/swe.20036.

973 Richards, P. G. (1995). Effects of auroral electron precipitation on topside ion outflows. *Cross-*
974 *Scale Coupling in Space Plasmas*, *93*, 121-126.

975 Schunk, R. W. (2000). Theoretical developments on the causes of ionospheric outflow. *Journal*
976 *of Atmospheric and Solar-Terrestrial Physics*, *62*(6), 399-420.

977 Schunk, R., and A. Nagy, *Ionospheres*, second ed., Cambridge University Press, Cambridge
978 Books Online, 2009.

979 Schunk, R.W., and W.J. Raitt, Atomic Nitrogen and Oxygen Ions in the Daytime High-Latitude
980 F-Region, J. Geophys. Res.: Space Physics, 85 (NA3), 1255–1272, 1980.

981 Seki, K., A. Nagy, C. M. Jackman, F. Crary, D. Fontaine, P. Zarka, P. Wurz, A. Milillo, J. A.
982 Slavin, D. C. Delcourt, M. Wiltberger, R. Ilie, X. Jia, S. A. Ledvina, M. W. Liemohn, and
983 R. W. Schunk (2015), A review of general physical and chemical processes related to
984 plasma sources and losses for solar system magnetospheres, *Space Sci. Rev.*, 1-63, doi:
985 10.1007/s11214-015-170-y.

986 Sojka, J.J., R.W. Schunk, and W.J. Raitt, Seasonal-Variations of the High-Latitude F Region for
987 Strong Convection, J. Geophys. Res.: Space Physics, 87 (NA1), 187–198, 1982.

Stebbings, R.F., W.L. Fite, and D.G. Hummer, Charge Transfer between Atomic Hydrogen and N^+ and O^+, The Journal of Chemical Physics, 33(4), 1226–1230, 1960.

Strangeway, R. J., Russell, C. T., Carlson, C. W., McFadden, J. P., Ergun, R. E., Temerin, M., Klumpar, D. M., Peterson, W. K., and Moore, T. E. (2000), Cusp field-aligned currents and ion outflows, *J. Geophys. Res.*, 105(A9), 21129– 21141, doi:10.1029/2000JA900032.

Strangeway, R.J., R.E. Ergun, Y.-J. Su, C.W. Carlson, and R.C. Elphic, Factors controlling ionospheric outflows as observed at intermediate altitudes, J. Geophys. Res.: Space Physics, 110 (A3), doi: 10.1029/2004JA010829, a03221, 2005.

Su, Y. J., Horwitz, J. L., Wilson, G. R., Richards, P. G., Brown, D. G., & Ho, C. W. (1998a). Self-consistent simulation of the photoelectron-driven polar wind from 120 km to 9 RE altitude. *Journal of Geophysical Research: Space Physics*, *103*(A2), 2279-2296.

Su, Y.-J., Horwitz, J. L., Moore, T. E., Giles, B. L., Chandler, M. O., Craven, P. D., Hirahara, M., and Pollock, C. J. (1998b), Polar wind survey with the Thermal Ion Dynamics Experiment/Plasma Source Instrument suite aboard POLAR, *J. Geophys. Res.*, 103(A12), 29305– 29337, doi:10.1029/98JA02662.

Tam, S.W.Y., T. Chang, V. Pierrard (2007). Kinetic modeling of the polar wind. Journal of Atmospheric and Solar-Terrestrial Physics, 69(16), 1984–2027. doi:10.1016/j.jastp.2007.08.006.

Trung, H.-S., M. W. Liemohn, and R. Ilie (2019). Steady state characteristics of the terrestrial geopauses. *Journal of Geophysical Research Space Physics*, 124, 5070-5081, https://doi.org/10.1029/2019JA026636.

Trung, H.-S., Liemohn, M. W. & Ilie, R. (2023). Momentum sources in multifluid MHD and their relation to the geopauses. Journal of Geophysical Research – Space Physics, 128, e2023JA031415. https://doi.org/10.1029/2023JA031415

Valek, P. W., Perez, J. D., Jahn, J. M., Pollock, C. J., Wüest, M. P., Friedel, R. H. W., ... & Peterson, W. K. (2002). Outflow from the ionosphere in the vicinity of the cusp. *Journal of Geophysical Research: Space Physics*, *107*(A8), SMP-13.

Wahlund, J. E., Opgenoorth, H. J., Häggström, I., Winser, K. J., & Jones, G. O. L. (1992). EISCAT observations of topside ionospheric ion outflows during auroral activity: Revisited. *Journal of Geophysical Research: Space Physics*, *97*(A3), 3019-3037.

Waite Jr, J. H., Nagai, T., Johnson, J. F. E., Chappell, C. R., Burch, J. L., Killeen, T. L., ... & Shelley, E. G. (1985). Escape of suprathermal O^+ ions in the polar cap. *Journal of Geophysical Research: Space Physics*, *90*(A2), 1619-1630.

Weimer, D.R., An improved model of ionospheric electric potentials including substorm perturbations and application to the Geospace Environment Modeling November 24, 1996, event, J. Geophys. Res.., 106, 407–416, doi:10.1029/2000JA000604, 2001a.

Weimer, D.R., Maps of ionospheric field-aligned currents as a function of the interplanetary magnetic field derived from Dynamics Explorer 2 data, J. Geophys. Res.: Space Physics, 106 (A7), 12,889–12,902, doi:10.1029/2000JA000295, 2001b.

Welling, D.T., and S.G. Zaharia, Ionospheric outflow and cross polar cap potential: What is the role of magnetospheric inflation?, Geophys. Res. Lett., 39 (23), doi: 10.1029/2012GL054228, 2012.

Welling, D. T., and M. W. Liemohn (2014). Outflow in global magnetohydrodynamics as a function of a passive inner boundary source, *J. Geophys. Res. Space Physics, 119*, 2691-2705, doi: 10.1002/2013JA019374.

Welling, D.T., and M.W. Liemohn (2016). The ionospheric source of magnetospheric plasma is not a black box input for global models J. Geophys. Res.: Space Physics, 121 (6), 5559–5565.

Welling, D.T., V.K. Jordanova, S.G. Zaharia, A. Glocer, and G. Toth (2011). The effects of dynamic ionospheric outflow on the ring current, J. Geophys. Res.: Space Physics, 116 (A15), A00J19, doi:10.1029/2010JA015642.

Welling, D.T., V.K. Jordanova, A. Glocer, G. Toth, M.W. Liemohn, and D.R. Weimer (2015a). The two-way relationship between ionospheric outflow and the ring current, J. Geophys. Res.: Space Physics, 120 (6), 4338–4353. doi:10.1002/2015JA021231

Welling, D.T., et al., (2015b). The Earth: Plasma Sources, Losses, and Transport Processes, Space Science Reviews, 192 (1-4), 145–208. doi:10.1007/s11214-015-0187-2

Welling, D.T., Barakat, A.R., Eccles, J.V., Schunk, R.W. and Chappell, C.R. (2016). Coupling the Generalized Polar Wind Model to Global Magnetohydrodynamics. In *Magnetosphere-Ionosphere Coupling in the Solar System* (eds C.R. Chappell, R.W. Schunk, P.M. Banks, J.L. Burch and R.M. Thorne). https://doi.org/10.1002/9781119066880.ch14

Whalen, B.A., S. Watanabe, A.W. Yau (1991). Observations in the transverse ion energization region. Geophys. Res. Lett. 18(4), 725–728. doi:10.1029/90GL02788

Wilson, G. R., Khazanov, G., & Horwitz, J. L. (1997). Achieving zero current for polar wind outflow on open flux tubes subjected to large photoelectron fluxes. *Geophysical research letters*, *24*(10), 1183-1186.

Wilson, G.R., D.M. Ober, G.A. Germany, and E J. Lund (2004). Nightside auroral zone and polar cap ion outflow as a function of substorm size and phase, J. Geophys. Res.: Space Physics, 109 (A2), doi:10.1029/2003JA009835.

Wiltberger, M. (2015).Review of Global Simulation Studies of Effect of Ionospheric Outflow on Magnetosphere-Ionosphere System Dynamics, Magnetotails in the Solar System. A. Keiling (ed.), 207, 373–392.

Wiltberger, M., W. Lotko, J.G. Lyon, P. Damiano, and V. Merkin (2010). Influence of cusp O^+ outflow on magnetotail dynamics in a multifluid MHD model of the magnetosphere, J. Geophys. Res., 115 (1), A00J05.

Winglee, R. M. (2000). Mapping of ionospheric outflows into the magnetosphere for varying IMF conditions. *Journal of Atmospheric and Solar-Terrestrial Physics*, *62*(6), 527-540.

Winglee, R.M., D. Chua, M. Brittnacher, G.K. Parks, and G. Lu (2002). Global impact of ionospheric outflows on the dynamics of the magnetosphere and cross-polar cap potential, J. Geophys. Res.: Space Physics, 107, 1237, doi:10.1029/2001JA000214.

Winglee, R.M., E. Harnett, and A. Kidder (2009). Relative timing of substorm processes as derived from multifluid/multiscale simulations: Internally driven substorms, J. Geophys. Res.: Space Physics, 114 (A), A09,213.

Winningham, J.D., and C. Gurgiolo (1982). De-2 photoelectron measurements consistent with a large scale parallel electric field over the polar cap, Geophys. Res. Lett., 9 (9), 977–979.

Wu, X. Y., Horwitz, J. L., Estep, G. M., Su, Y. J., Brown, D. G., Richards, P. G., & Wilson, G. R. (1999). Dynamic fluid-kinetic (DyFK) modeling of auroral plasma outflow driven by soft electron precipitation and transverse ion heating. *Journal of Geophysical Research: Space Physics*, *104*(A8), 17263-17275.

Yau, A.W., P.H. Beckwith, W.K. Peterson, and E.G. Shelley (1985). Long-term (solar cycle) and seasonal variations of upflowing ionospheric ion events at DE 1 altitudes, J. Geophys. Res., (ISSN 0148-0227), 90 (A7), 6395–6407.

Yau, A.W., W.K. Peterson, and E.G. Shelley (1988). Quantitative parameterization of energetic ionospheric ion outflow, Washington DC American Geophysical Union Geophysical Monograph Series, pp. 211–217.

Yau, A. W., Whalen, B. A., Abe, T., Mukai, T., Oyama, K. I., & Chang, T. (1995). Akebono observations of electron temperature anisotropy in the polar wind. *Journal of Geophysical Research: Space Physics*, *100*(A9), 17451-17463.

Yau, A. W., & André, M. J. S. S. R. (1997). Sources of ion outflow in the high latitude ionosphere. *Space Science Reviews*, *80*(1-2), 1-25.

Yau, A.W., E. Drakou, M.J. Greffen, D.J. Knudsen, and E. Sagawa (1998). Radio-Frequency Ion Mass Spectrometer Measurements of Ion Composition, Velocity and Temperature: the EXOSD Suprathermal Mass Spectrometer, Geophysical Monograph Series, vol. 102, American Geophysical Union, Washington, D.C.

Yau, A.W., T. Abe, and W. Peterson (2007). The polar wind: Recent observations, Journal of Atmospheric and Solar-Terrestrial Physics, 69 (16), 1936–1983, doi:10.1016/j.jastp.2007.08.010.

Yizengaw, E., Moldwin, M. B., Dyson, P. L., Fraser, B. J., & Morley, S. (2006). First tomographic image of ionospheric outflows. *Geophysical research letters*, *33*(20).

Young, D.T., H. Balsiger, and J. Geiss (1982). Correlations of magnetospheric ion composition with geomagnetic and solar activity, J. Geophys. Res., 87, 9077–9096, doi:10.1029/JA087iA11p09077.

Yu, Y., and A.J. Ridley (2013a). Exploring the influence of ionospheric O^+ outflow on magnetospheric dynamics: Dependence on the source location, J. Geophys. Res.: Space Physics, 118(4), 1711–1722, doi:10.1029/2012JA018411.

Yu, Y., and A.J. Ridley (2013b). Exploring the influence of ionospheric O+ outflow on magnetospheric dynamics: The effect of outflow intensity, J. Geophys. Res.: Space physics, 118(9), 5522–5531, doi:10.1002/jgra.50528.

Zeng, W., & Horwitz, J. L. (2007). Formula representation of auroral ionospheric O+ outflows based on systematic simulations with effects of soft electron precipitation and transverse ion heating. *Geophysical research letters*, *34*(6).

1110 Zhou, X.W., C.T. Russell, G. Le, S.A. Fuselier, and J.D. Scudder (2000). Solar wind control of
1111 the polar cusp at high altitude, J. Geophys. Res.: Space Physics, 105 (A1), 245–251,
1112 doi:10.1029/1999JA900412.
1113